Theor. Comput. Fluid Dyn. (2020) 34:301–332
https://doi.org/10.1007/s00162-020-00523-1

ORIGINAL ARTICLE

Kaustav Pradhan · Abhijit Guha

A systematic study of blockage in three-dimensional branching networks with an application to model human bronchial tree

Received: 14 June 2019 / Accepted: 24 March 2020 / Published online: 12 June 2020

Abstract A major aim of the present study is to understand and thoroughly document the fluid dynamics in three-dimensional branching networks when an intermediate branch is partially or completely obstructed. Altogether, 26 different three-dimensional networks each comprising six generations of branches (involving 63 straight portions and 31 bifurcation modules) are constructed and appropriately meshed to conduct a systematic study of the effects of varying the locations of a blockage of a given relative extent and varying the extent of a blockage at a fixed location. The side-by-side consideration of two branching configurations (in-plane and 90° out-of-plane) gives a quantitative assessment of the dependence of flow alteration due to blockage on the three-dimensional arrangement of the same individual branches. A blockage in any branch affects the flow in both downstream and upstream branches. The presence of a blockage can make three-dimensional asymmetric alteration to the flow field, even when the blockage itself is geometrically symmetric. The overall mass flow rate entering the network is found to remain nearly unaltered if a blockage is shifted within the same generation but is progressively reduced if the blockage is shifted to upstream generations. A blockage anywhere in the network increases the degree of mass flow asymmetry $\delta_{\mathrm{G}n}$ in any generation. The order of magnitude disparity in $\delta_{\mathrm{G}n}$ between the in-plane and out-of-plane configurations, characteristic of unobstructed networks, can be significantly reduced in the presence of a single blockage. The present three-dimensional computations show that the effects of blockage on the mass flow distribution in a large network are complex, often non-intuitive and sometimes dramatic, and cannot be captured by any simple one-dimensional model.

Keywords Fluid dynamics · CFD · Branching network · Blockage

1 Introduction

A study of the flow in branched networks is of fundamental and practical importance since such networks are often encountered in biological systems and are increasingly being contemplated for engineering applications. As an example, the knowledge of particle transport and deposition in the bronchial tree, which in turn depends on the fluid flow field, is important for understanding (and perhaps controlling) the causation of certain diseases and for targeted drug delivery. A lucid but comprehensive description of the flow of fluid and particles in the human bronchial tree is given by Guha [1]. Branched networks based on fractal (or other) algorithms may find application in micro- or macro-systems designed for the exchange of mass or energy. Ref. [2] discusses an example of a novel heat exchanger for a hypersonic engine, its bio-inspired design being based on the fish-gill morphology. The present paper undertakes a systematic study about how the fluid mechanics in a three-dimensional branching network is modified, sometimes dramatically, due to the presence of a blockage

Communicated by Jeff D. Eldredge.

K. Pradhan · A. Guha (✉)
Mechanical Engineering Department, Indian Institute of Technology Kharagpur, Kharagpur 721302, India
E-mail: a.guha@mech.iitkgp.ac.in

somewhere in the network. Our emphasis is on understanding the generality of the fluid dynamics; studying special morphological or physiological features of a biological system is not the purpose of the present study. We have adopted generalized geometric models [3] of the human bronchial tree as example geometries for the numerical simulations and analysis, but the results will also be useful in understanding the flow in engineered branching networks.

An obstruction in the flow path may be caused by structural changes in the branch wall or significant accumulation of extraneous matter. As an example, such blockage in the human airways may give rise to chronic obstructive pulmonary disease (COPD), which may severely restrict the respiratory airflow in the patient. Stenosis may bring similar changes in the cardiovascular network. Similarly, blocked flow passages in micro-channel networks for electronic cooling may lead to inefficient cooling and consequent damage to the device. Hence, it is necessary to assess the effects of (partial or complete) obstructions in the flow path in branching networks.

There exists a rich literature that deals with many aspects of unobstructed airflow and particle deposition in branching geometries. In two recent publications [4,5], the flow in three-dimensional branching networks comprising six generations of branches is comprehensively analysed, specifying and systematizing the complex primary flow field and quantifying the generation and evolution of secondary motion. Most of the previous studies had used fewer generations. Zhao et al. [6–8] performed experiments for flow in a single bifurcation and generated numerical results for the same geometry. Tadjfar and Smith [9] studied the flow in a single mother tube of circular cross section branching into two equal but diverging daughter tubes of semi-circular cross section using direct numerical simulations (DNS) and slender flow modelling. Kang et al. [10] analysed the effect of geometric variations on the pressure loss across a single bifurcation. In a recent publication [11], the fluid dynamics of a bifurcation has been thoroughly studied, establishing the mechanisms of loss production in a bifurcation and quantifying the enhanced loss incurred in straight pipes following a bifurcation as compared to that in a similar straight pipe in isolation. The airflow in three generations of the bronchial tree was studied by Liu et al. [12], Comer et al. [13], Wilquem and Degrez [14] and Heistracher and Hofmann [15]. Leong et al, [16] studied secondary flow in a double bifurcation, and Fresconi and Prasad [17] studied the same in a four-generation network. Since a single computation covering the entire bronchial tree is computationally resource intensive, previous researchers [18,19] developed modular approaches (in which the bronchial tree is segmented into small units comprising three or four generations of branches) but did not demonstrate the effects of such segmentation on the overall accuracy of the results. Most of the above-mentioned studies are based on generalized models of the bronchial tree.

Comerford et al. [20] described a 3D–1D coupled model of the bronchial tree, wherein the flow conditions at the outlets of the 3D domain (representing the first few generations of the bronchial tree starting at the trachea) are derived from a 1D model of the downstream networks. Ismail et al. [21] proposed a total lung model based on "0D" [21] airways. Following these studies, Kannan et al. [22] developed a quasi-3D wire model for the bronchial tree. Recently, Pozin et al. [23,24] used a 3D–0D coupled tree-parenchyma model to study lung ventilation. The challenges that a 1D model faces are summarized later in the present work. Studies of fluid flow and particle deposition in patient-specific CT scanned respiratory airways [25–28] and in computer generated asymmetric lung models [29,30] have also been carried out by some researchers. However, generalized geometric models are normally used in studies where understanding general fluid dynamic features is the priority.

The existing literature on the airflow in obstructed human airways is rather thin. Yang et al. [31] studied blockage in the second and third generations in a three-generation symmetric planar model of the human bronchial airways, and Yang et al. [32] did the same for a four-generation symmetric planar model; only the case of 75% blockage was considered (whereas a systematic variation of the extent of blockage is included in the present paper). Yang et al. concluded that consideration of only a few generations (such as 3) is a serious limitation in the studies of blockage or COPD. The effect of asthmatic constrictions in the flow path for a three-generation paediatric airway model was studied by Longest et al. [33]. Farkas and Balashazy [34] performed simulations to predict the effect of tumours and blockages on the flow field and deposition efficiencies in three-generation (G2–G4) symmetric planar Weibel's geometry.

Our aim is to make a generalized fluid dynamic study of the effects of blockage in a three-dimensional branching network. A few of the specialities of the present study are summarized below.

1. A six-generation branching network is considered for all simulations presented in the current paper. Since the number of branches increases rapidly with number of generations according to the formula $2^n - 1$, where n is the number of generations, the computational challenge undertaken here is considerable. The

Table 1 Dimensions for the first six generations of the human bronchial tree according to Weibel [3]

Generation number	Diameter d_{branch} (mm)	Length L (mm)
G0 (trachea)	18.00	120.00
G1	12.20	47.60
G2	8.30	19.00
G3	5.60	7.60
G4	4.50	12.70
G5	3.50	10.70

six-generation network comprises 63 branches and 31 bifurcation modules, whereas most other reported studies were conducted in a three-generation network comprising only 7 branches.
2. Side-by-side with the planar network, the effects of blockage in a non-planar, space-filling three-dimensional arrangement of the same individual branches are studied here, for the first time. This gives a quantitative assessment of the dependence of flow alteration due to blockage on the three-dimensional arrangement of the same individual branches.
3. A direct consequence of adopting a six-generation model is that a meaningful study of the effects of systematically varying the location of a given blockage has been possible. This allows one to understand both upstream and downstream effects of a blockage.
4. For each alteration of the extent of blockage at a fixed location and the location of a blockage of a fixed size, the internal intricate three-dimensional flow passages change, and consequently, the entire network needs to be meshed again. For the specification and systematization of the effects of blockage on the flow field, altogether 26 different three-dimensional networks (each comprising six generations of branches) are constructed and appropriately meshed. This makes the present study comprehensive.
5. Instead of the often used velocity inlet condition, the driving potential across the network is kept fixed, which makes the study of blockage physically more realistic but computationally more challenging.
6. Great emphasis is placed on the accuracy and precision of the computed results. Fine meshes involving more than 30 million computational cells are used to capture fine flow details. Double-precision arithmetic is used.
7. The effects of changing location and extent of blockage on the flow through each of the 63 branches are meticulously documented. From these detailed observations, generalized principles have been drawn to an extent that was feasible; a summary of such generalizations is given in the Conclusion.
8. It is shown that neither the quantitative information nor all qualitative characteristics can be deduced from intuition or determined by simple one-dimensional models.

2 Geometric details and philosophy of design of computational cases

A three-dimensional idealized model of the bronchial tree network is constructed by successively connecting cylindrical sections representing the bronchial airways of a particular generation with those of the next generation through bifurcation modules [4]. A particular generation in the network is referred here by the symbol Gn, where the index n denotes the generation number and progressively takes the integer values 0, 1, 2, etc. The six-generation network considered here therefore consists of generations G0 to G5. The dimensions of the branches considered in this study are shown in Table 1. The bifurcation angle (angle between two daughter branches emanating from the same mother branch) is set to 70° for all generations. All the branches are denoted by 'GnBk', where 'Gn' denotes the generation to which the branch belongs while 'Bk' denotes the branch number in a particular generation. The start and end planes of the branches are denoted by 'GnSk' and 'GnPk', respectively. Two types of three-dimensional arrangement of the same branches have been considered here, giving rise to two configurations, viz. in-plane and out-of-plane.

Figure 1 shows a three-dimensional view of the branching network [3] with the branches arranged in the in-plane configuration. For this arrangement of branches, the centrelines of all the branches lie on a single plane (which is denoted by the term 'meridional plane' [4]). Although this configuration is planar, the three-dimensional internal flow passages makes it necessary to perform three-dimensional CFD simulations for determining the fluid flow field. The branches in a generation in the in-plane configuration are numbered from left to right as shown in Fig. 1.

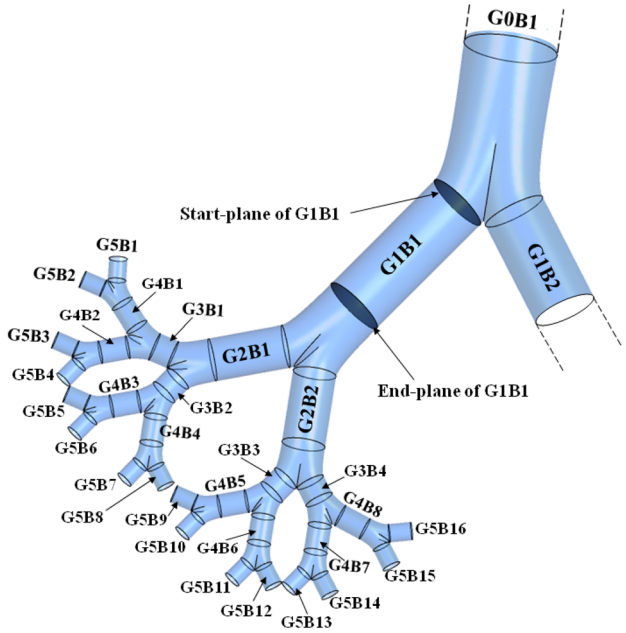

Fig. 1 Six generations (G0–G5) of a symmetric model of the human bronchial tree [3]; in-plane configuration (Only half of the network is shown here. Simulations are run for the entire network)

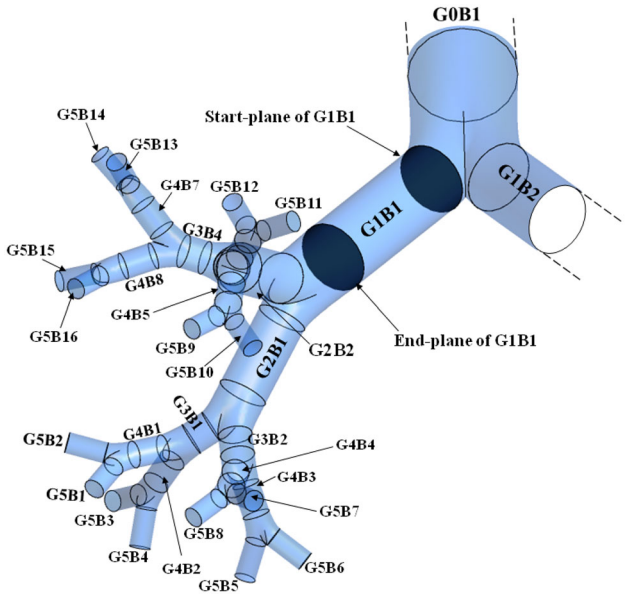

Fig. 2 Six generations (G0–G5) of a symmetric model of the human bronchial tree [3]; out-of-plane configuration (Only half of the network is shown here. Simulations are run for the entire network)

A three-dimensional view of the six-generation branching network [3] with the branches arranged in the out-of-plane configuration is shown in Fig. 2. The dimensions of the cylindrical sections and geometries of the bifurcation modules in this configuration are the same as those of the in-plane configuration, but they are connected differently. Each flow unit [4] comprising a bifurcation module, a preceding mother branch and two succeeding daughter branches (all of which must have centrelines lying on a single plane) lies at 90° to its preceding flow unit. Hence, this arrangement of the branches is referred to as the 90° out-of-plane configuration. Figure 2 provides a pictorial guide for the nomenclature used for the out-of-plane configuration.

The present study is aimed at understanding the effect of a (partial/complete) blockage in the flow path in one of the branches of the G0–G5 network on the overall flow characteristics. It is assumed here that the

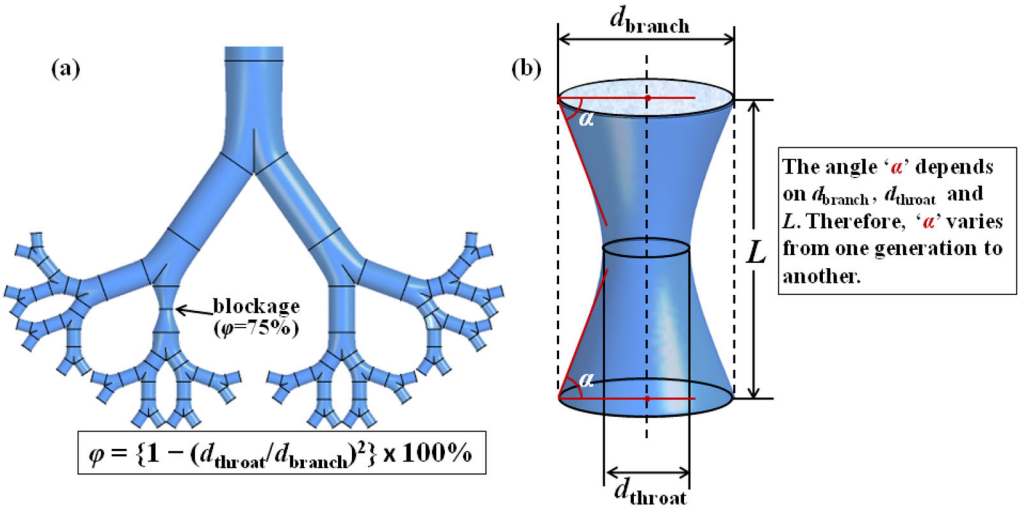

Fig. 3 Geometric details of the type of obstruction considered in the present study **a** a six-generation in-plane network with a 75% blockage in G2B2, **b** enlarged view of the blockage with geometric parameters

blockage occurs in the straight portion of a branch and is a result of a symmetric narrowing of the flow area, while maintaining the circular shape, as shown in Fig. 3. (In the biological context, the narrowing may be caused by the inflammation of the branch walls.) The percentage of the total cross-sectional area of a branch that is blocked at the throat section of a blockage is termed as extent of blockage (φ) and is given by the expression

$$\varphi = \left(1 - \frac{d_{\text{throat}}^2}{d_{\text{branch}}^2}\right) \times 100. \tag{1}$$

The ratio $d_{\text{throat}}/d_{\text{branch}}$ is varied from 1 to 0 such that φ varies from 0% (no blockage) to 100% (complete blockage). The present study considers the presence of a single blockage in the network, with variation of its extent and location. One case of partial blockage in the network is shown in Fig. 3a, and an enlarged view of the blockage geometry is shown in Fig. 3b. For the case of complete blockage, the flow does not pass the blockage and hence the branches downstream of the blockage are not considered in the simulations. The branching networks shown in Figs. 1 and 2 do not have any blockages in the flow path ($\varphi = 0$), and they are referred to as unobstructed networks in this paper.

The three-dimensional arrangement of the branches and bifurcation modules in the out-of-plane arrangement makes the complexity of the internal geometry immediately obvious. It must be appreciated that although the centrelines of all branches and their connecting bifurcation modules in the in-plane configuration lie on a single plane, the internal flow passages are still three-dimensional and complex [4]. The symmetry in the geometry of any two branches in the adopted symmetric model does not automatically imply symmetry in the flow field in those two branches. The combined effects of flow path curvature in the bifurcation module, flow division at a bifurcation and inertia of the flow result in non-uniform flow distribution and complex fluid dynamics even in the geometrically symmetric model. It is, however, shown in Ref. [4] that the flow features in the in-plane configuration are symmetric about the longitudinal symmetry plane, and for every branch there exists one (and one only) more branch (the homologue) in the same generation in which the flow solution is replicated in entirety. Similarly, it is established in Ref. [4] that the flow features in the out-of-plane configuration are symmetric about the longitudinal and transverse symmetry planes, and for every branch there exist three (and three only) more branches (the homologues) in the same generation in which the flow solution is replicated in entirety. The presence of blockage in any branch removes this symmetry and makes it necessary to determine the flow field in the entire network (since the flow field in any branch of an obstructed network is different from that in any other branch). However, the effects of a blockage in a branch and those for an identical blockage in its homologous branches of the unobstructed network are found to be identical.

For conciseness, all branches originating from G1B1 are collectively named below as sub-network L and all branches originating from G1B2 are named as sub-network R. For the out-of-plane network, the sub-network L

can be thought of being divided into two parts L1 and L2. Since the effects of a blockage in a branch and those for an identical blockage in its homologous branches (1 in in-plane due to twofold symmetry, 3 in out-of-plane due to fourfold symmetry) of the unobstructed network would be identical, a study of blockage in branches of sub-network L for the in-plane configuration and that in branches of sub-network L1 for the out-of-plane configuration would be representative for the entire network. Therefore, computations are performed for a blockage ($\varphi = 75\%$) in branches of generations G2 (G2B1 and G2B2), G3 (G3B1, G3B2, G3B3 and G3B4) and G4 (G4B5 and G4B6) of the in-plane configuration, and, in branches of generations G2 (G2B1), G3 (G3B1 and G3B2) and G4 (G4B1, G4B2, G4B3 and G4B4) of the out-of-plane configuration. The effect of φ is studied by constructing separate geometries for a blockage in G2B2 in the in-plane configuration and a blockage in G2B1 in the out-of-plane configuration, with φ set to 0% (unobstructed network), 25%, 50% and 100% (complete obstruction). Additionally, out-of-plane networks with 75% blockage in G2B2, G3B3 and G4B6 are also simulated for direct comparison with their in-plane counterparts. Altogether, 26 separate three-dimensional geometries of the six-generation network are constructed and simulated in this study to account for the variation of the three-dimensional arrangement of the branches (in-plane and out-of-plane), location of the obstructed branch and the extent of obstruction,

2.1 Summary of solution methodology

The details of the computational method and validation are given in Ref. [4]. Here, we only provide a summary to save space. The present analysis considers steady, laminar, incompressible flow, the governing equations being:

Mass conservation:

$$\nabla \cdot \vec{v} = 0 \tag{2}$$

Momentum conservation:

$$\rho(\vec{v} \cdot \nabla)\vec{v} = -\nabla p + \mu \nabla^2 \vec{v} \tag{3}$$

Here, $\vec{v}$ represents the velocity vector of the fluid, ρ is the fluid density, p is the static pressure, and μ is the dynamic viscosity of the fluid. The effects of gravity and oscillating boundary condition [35,36] are not considered here. Air is considered to be the working fluid and accordingly, ρ and μ are taken as $1.225\,\mathrm{kg/m^3}$ and $1.7894 \times 10^{-5}\,\mathrm{kg/(ms)}$, respectively, for all results reported in this paper.

The three-dimensional models for the branching networks are built in SolidWorks 2010 [37], and the meshing and numerical simulations are performed on the ANSYS Workbench [38] using the ANSYS Mesh Modeler and a finite-volume-based CFD solver FLUENT, respectively. The no-slip and no-penetration conditions are applied on the walls of the branches which are assumed to be rigid [6–19]. A consideration of the flexibility of the branch walls would require the use of fluid–structure interaction (FSI) simulations, and then the size of the branching tree would need to be restricted, thereby compromising the detailed generality of the fluid dynamics of blockage in a large branching tree, on which we have placed the emphasis in the present study by using a six-generation network. Moreover, for an engineered branching network, the rigid wall assumption may be the realistic one.

A large number of papers [8–16,19,25–34,39] employ the pressure boundary condition at the outlets since it can accommodate the non-uniform flow distribution arising in the network. Moreover, for an engineered branching network, the outlet pressure assumption may be the realistic one. We have adopted this exit boundary condition for the present study. The 'Pressure Outlet' boundary condition feature of FLUENT is used to specify a zero gauge pressure at the ends of the branches of generation G5 (i.e. the outlets of the computational domain).

A systematic and detailed study was undertaken to specify the appropriate inlet boundary condition. It is anticipated that with a given value of available driving potential (i.e. the decrease in total pressure between the inlet and its mass flow-averaged value at the outlets) across a real bronchial network, the presence of blockages would reduce the total mass flow rate through the network. It is established here that this realistic condition is achieved, as a good approximation, by keeping the inlet total pressure and outlet static pressures fixed as blockages of varied extent and location are introduced in the network. It is to be noted that the often-used velocity inlet condition, which is computationally less challenging, would have made physical interpretation of computed results quite awkward since fixing the inlet velocity (i.e. total mass flow rate) would imply a greater value of driving potential in the presence of blockages as compared to the flow through an unobstructed network. Detailed results of this study are not presented here for brevity.

Table 2 Details of the grid independence study for the in-plane configuration of branching network comprising generations G0–G5 performed at $p_{\text{total,in}} = 2.7\,\text{Pa}$

Number of elements in mesh	r_{grid}	ε_{rms}	GCI
542,115 (coarse)–1,838,556 (medium)	1.502	0.0411	0.0982
1,838,556 (medium)–6,384,237 (fine)	1.514	0.0111	0.0258
6,384,237 (fine)–30,942,837 (very fine)	1.692	0.0108	0.0176

An unstructured mesh with a sufficiently large number of tetrahedral elements is used in the present study. The pressure-based solver available in FLUENT is used. All transport equations are discretized with second-order accuracy in space. The diffusion terms are discretized using central difference scheme. The advection terms are discretized using the second-order upwind scheme. This reduces the numerical diffusion associated with an unstructured mesh [40]. A segregated implicit [41] solver is used to solve the resulting system of discretized equations. The solver uses a time-marching technique [42,43] to achieve a steady state solution as the limiting process of an unsteady simulation. The SIMPLE algorithm is employed in coupling the velocity and pressure. The convergence criterion is set at 10^{-8} for the scaled residuals of the continuity equation as well as the three momentum equations. Double-precision arithmetic is used.

A comprehensive grid independence study has been performed for the branching networks following the methodology suggested by Roache [44] and Celik et al. [45]. The details of the meshes with results of the grid independence test for the in-plane configuration are tabulated in Table 2. Using about 30 million computational cells, the value of the apparent order of discretization (q) is found to be 1.92 for in-plane and 2.05 for out-of-plane configurations, with respective GCI (grid convergence index) being 1.76% and 2.18%. These figures are indicative of the achievement of grid-independent solution. The present numerical method is validated through comparisons with the experimental results of Zhao and Lieber [6]. The present computations compare well with experiments at various values of inlet Reynolds number ($\text{Re} \equiv 2\rho U R_{\text{G0}}/\mu$, where R_{G0} is the radius of the branch G0B1 and U is the average velocity in that branch), the agreement being superior to that between the computations of Comer et al. [13] and the same experiments. This establishes the capability of the present numerical method in accurately capturing the complex fluid dynamics in three-dimensional branching networks comprising several generations of branches.

In the present study, simulations are performed for both in-plane and out-of-plane configurations for various values of the inlet total pressure. Each value of inlet total pressure corresponds to the mass flow-averaged [46] inlet total pressure obtained from the CFD solution for the unobstructed network with specified inlet Reynolds number (i.e. inlet velocity) in the range $400 \leq \text{Re} \leq 1200$. The flow downstream of the extra-thoracic complexities (i.e. from the beginning of the straight tracheal tube) is considered in the present fluid dynamic study. Considering a tidal volume of 0.5 L and tracheal diameter of 1.8 cm, this Re range generally corresponds to normal breathing rates in an adult human under resting condition [47].

3 Results and discussion for the in-plane configuration

It is explained in Sect. 2 that it is necessary and sufficient to determine the effects of a blockage in branches lying in one half of the network (denoted as sub-network L in Sect. 2) for the in-plane configuration, though for a particular blockage the flow field in the entire network needs to be simulated. An initial CFD simulation, using inlet velocity condition, determined that an inlet Reynolds number of 1000 requires $p_{\text{total,in}} = 2.7\,\text{Pa}$ in unobstructed in-plane G0–G5 network. This total pressure at inlet is specified in the simulations described in this section so as to keep the driving potential constant for all cases of blockage.

3.1 General effects of blockage on flow field

Some overall features of an example flow solution are shown in Fig. 4 in which the effects of 75% blockage in G2B2 (which lies in the maximum flow path in the unobstructed network) are considered. Cross sections A, B and C correspond to the start plane, throat (for obstructed branch) and end plane, respectively, of branch G2B2. The representational convention is adopted such that the downstream bifurcation ridge appears as vertical line in the diagram and the primary flow is towards the reader. Figure 4 shows that the average velocity at the start plane of the branch (station A) is considerably reduced in the presence of a blockage indicating a reduction in

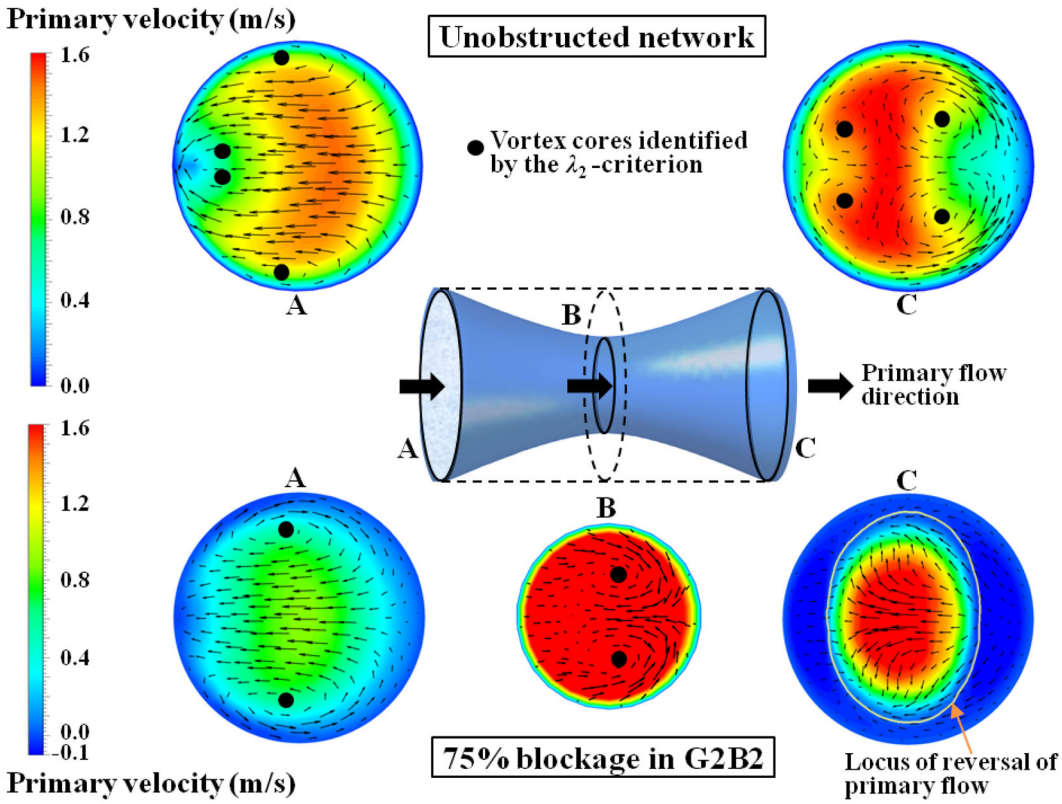

Fig. 4 Contours of primary velocity with superposed secondary velocity vectors at specified locations of branch G2B2 in the unobstructed network and in the presence of a 75% blockage in the same branch; in-plane configuration (The length of the vectors on any cross-sectional plane indicates the secondary velocity scaled by the respective maximum secondary velocity on that plane)

the mass flow rate in the branch due to the blockage. In the diverging portion (between B and C) of the blocked branch, flow separation near the walls results in a jet-like flow stream at the centre of the cross section with reversed flow in the peripheral region. The velocity field in the unobstructed branch does not show any such flow reversal. It is interesting to note that the maximum velocity at the end plane (station C) of the obstructed branch is significantly greater than that at its start plane (station A). This indicates that the presence of a blockage increases the cross-sectional non-uniformity in the velocity distribution in the blocked branch.

The secondary velocity vectors shown in Fig. 4 indicate that the presence of a blockage in a branch significantly alters the nature of secondary motion in that branch. The upstream effects of the blockage is demonstrated by the difference in the secondary flow pattern at station A; the four-vortex pattern at the start plane of the branch in the unobstructed network gives way to a two-vortex Dean-type circulation in the blocked branch. The downstream effects of the blockage can be seen by comparing the flow field at station C. The four-vortex system at station C in the unobstructed network (discussed in detail in Ref. [5]) is replaced by a secondary flow pattern which does not show any well-defined vortices in the blocked branch. A feature of the Dean-type circulation is present in the central region of the cross section of the blocked branch in that the fluid is seen to move towards the inner edge (towards left wall in the diagram) which is an expected result of curvature; but instead of forming any vortical structure, fluid from all regions in the cross section appear to converge to two points (which are symmetrically located about the horizontal diameter). In the present study, the λ_2-criterion [48] has been used as a supplemental method for locating the cores of the vortices in the flow field. According to this criterion, any point in the flow field, for which $\lambda_2 < 0$, is part of a vortex. Here, λ_2 refers to the median eigenvalue of the tensor $S^2 + \Omega^2$, where S is the symmetric part and Ω is the anti-symmetric part of the velocity gradient tensor.

Figure 5 shows the evolution of the flow field downstream of the blockage in G2B2, revealing at least three important effects of blockage in a large network. (i) For a significant blockage somewhere (75% in G2B2 in the chosen example), the recirculation regions developed in the diverging section immediately downstream of

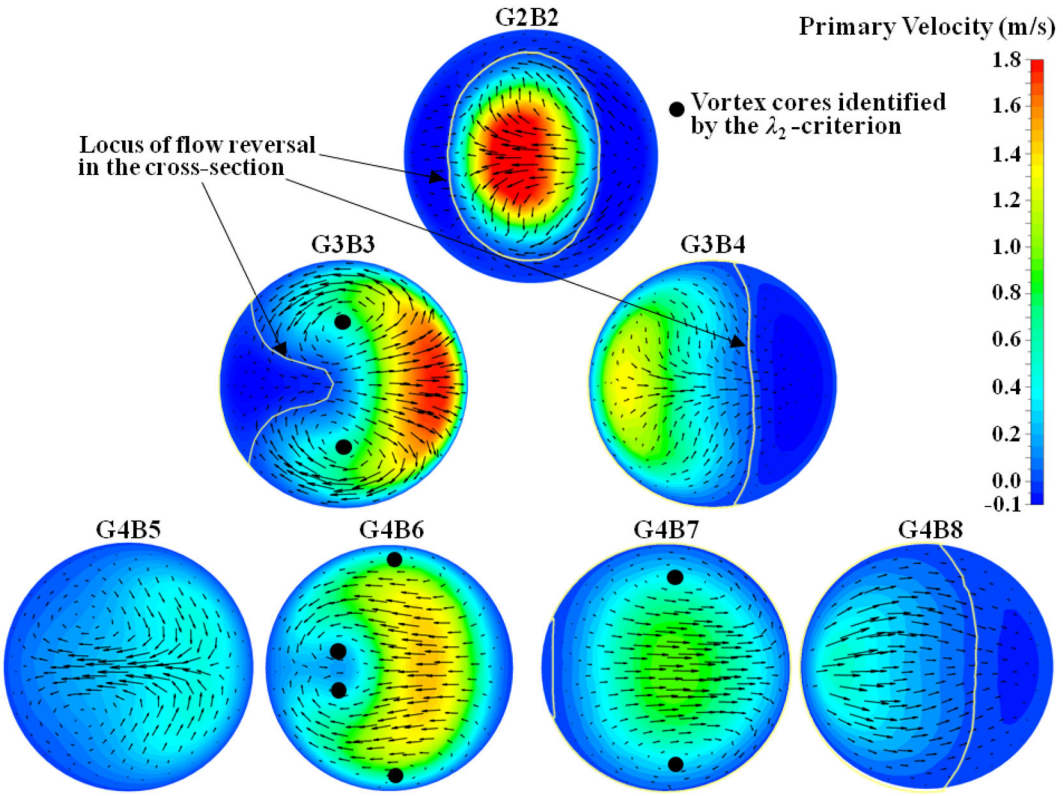

Fig. 5 Contours of primary velocity with superposed secondary velocity vectors at end planes of the named branches for 75% blockage in G2B2; in-plane configuration (The length of the vectors on any cross-sectional plane indicates the secondary velocity scaled by the respective maximum secondary velocity on that plane. The closed curves are constructed through post-processing to clearly demarcate two regions with opposite directions of primary flow)

the blockage (which is shown in Fig. 4) are found to persist in both daughter branches (G3B3 and G3B4), and even in branches further downstream. (ii) It is interesting to note in Fig. 5 that recirculation regions persist in G4B7 and G4B8, but are absent in G4B5 and G4B6. This may be attributed to the greater expanse of the recirculation region in G3B4 than that in G3B3. One physical implication of these observations is that, following the separation in the blocked branch, the reattachment lengths along various flow paths are different, (iii) It is shown in Ref. [4] that even for an unobstructed network, there are large differences in the mass flow rates through the G4 branches: the branches G4B6 and G4B7, being aligned with their grandmother G2B2, receive significantly greater mass flow rates than G4B5 and G4B8. This asymmetry among the G4 branches is accentuated by the formation of the central fluid jet in the blocked branch (G2B2) and the resulting highly skewed velocity distributions in G3B3 and G3B4 shown in Fig. 5.

It is shown in Ref. [5], that in the unobstructed network, there are four vortices (two Dean and two anti-Dean) in G2B1 and G2B2, two Dean-type vortices in all branches of G3 and in seven of the eight branches of G4 in sub-network L (while part length of one branch contains four vortices, though only two vortices are seen at the end plane of this branch also). Figure 4 shows that the presence of blockage removes any vortical pattern at the end plane of the blocked branch (G2B2). Figure 5 shows that this vortex-free secondary motion continues in G3B4 but a two-vortex system with Dean-type circulation develops in G3B3. While the mass flow rates in G4B5 and G4B8 are smaller than those in their sisters even in an unobstructed network, the disparity increases when their grandmother (G2B2) is partially blocked. As a consequence, Fig. 5 shows that there is no vortical structure in G4B5 and G4B8, but G4B6 shows the presence of a four-vortex system while G4B7 shows a two-vortex system with typical Dean-type circulation. The presence of blockage therefore significantly alters the secondary flow patterns in the downstream branches.

Figure 6 shows the effects of a 75% blockage in G2B2 on the distribution of magnitude of secondary velocity $|\vec{v}_S|$ at the start planes of branches G2B2, G3B3, G3B4, G4B5, G4B6, G4B7 and G4B8. (Since a bifurcation module creates secondary motion while a straight portion attenuates it [5], a good cross-sectional

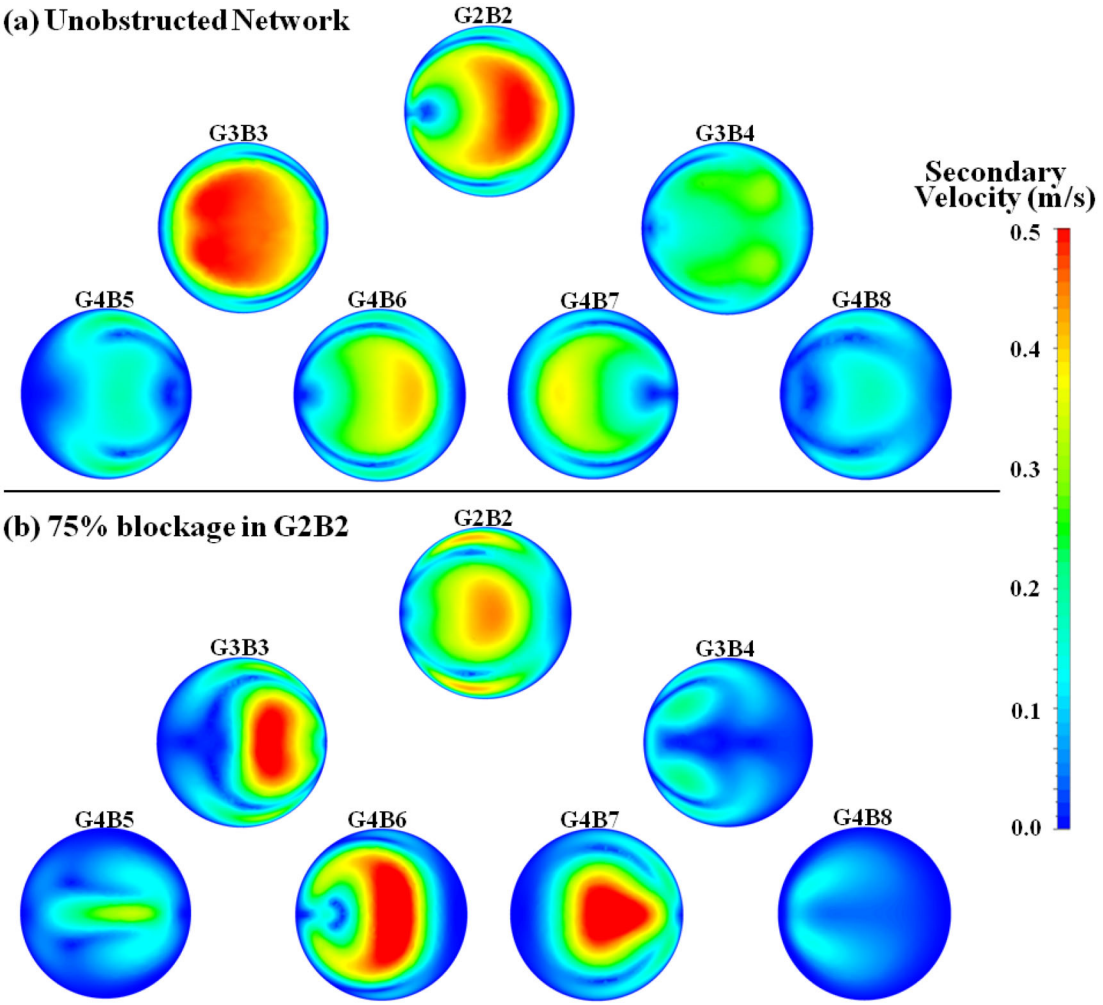

Fig. 6 Effect of blockage on the magnitude of secondary flow at the start planes of the blocked branch and its downstream branches; in-plane configuration

plane for the study of magnitude of secondary motion is the start plane of a branch.) The reduced magnitude of primary flow in the blocked branch (Fig. 4) results in a decrease in the maximum (and average) secondary velocity at the start plane of G2B2 as shown in Fig. 6. Although the average secondary velocity in G3B3 and G3B4 are significantly reduced in the presence of the blockage in G2B2, the maximum value of $|\vec{v}_S|$ in G3B3 is found to increase. This indicates that the blockage increases the cross-sectional inhomogeneity in the secondary velocity distribution in G3B3. Moreover, the blockage significantly increases the difference in the average secondary velocity among the G4 branches downstream of the blocked branch. It is interesting to note that although the average secondary velocity in G3B4 is much smaller than that in G3B3, the bifurcation module connecting G3B4, G4B7 and G4B8 generates considerable fresh secondary motion such that the average secondary velocity in G4B7 is comparable to that in G4B6.

Although not graphically displayed here, the same computations for the blockage in G2B2 reveal an increased secondary motion in the downstream branches of G2B1, due to the increased mass flow rate in G2B1. However, the qualitative nature of the secondary flow field in G2B1 and its downstream branches are not affected by a blockage in G2B2. Therefore, it may be inferred that a blockage in a branch considerably alters the secondary flow features in itself and its downstream branches, but does not significantly affect the qualitative features of the secondary flow in its sister and the downstream branches of the sister.

Table 3 Effect of extent of blockage φ on the drops in static pressure and total pressure across the network, and the total mass flow rate in the network for inlet gauge total pressure $p_{\text{total,in}} = 2.7$ Pa; in-plane configuration

Blockage position	Extent of blockage φ (%)	Drop in static pressure across network (Pa)	Drop in total pressure across network (Pa)	Mass flow rate through network (10^{-5} kg/s)
No blockage	0	2.281	2.073	25.34
G2B2	25	2.288	2.077	25.14
G2B2	50	2.311	2.089	24.41
G2B2	75	2.371	2.088	22.34
G2B2	100	2.435	1.993	20.10

3.2 Effects of the extent of blockage on velocity and mass distributions

We now consider the effect of the extent of blockage (φ) on the flow pattern and mass flow distribution in the network. φ values of 0% (no blockage), 25%, 50%, 75% and 100% (complete blockage) in G2B2 are considered. As a result of the location of the branch G2B2, both upstream and downstream effects of a blockage can be studied well here. Table 3 shows the variation with φ of the drop in static pressure and total pressure across the six-generation network as well as the overall mass flow rate in the network for a specified total pressure at the inlet (see Sect. 2.1).

Figure 7 shows the variation with φ of the velocity field on the meridional plane and mass flow distribution up to generation G4 when a blockage occurs in G2B2. It is found that significant quantitative changes take place both upstream and downstream of the blocked branch, and in all branches of both sub-networks (L and R), though the qualitative flow features in sub-network R remain essentially the same as in unobstructed flow. A blockage in G2B2 leads to an increase in mass flow rate in G1B2 and to a reduction of greater magnitude in G1B1 (mother of G2B2) resulting in a decrease in the overall mass flow rate through the network. The rate of decrease in overall mass flow rate increases with an increase in the extent of blockage φ (Table 3 and Fig. 7). Ref. [4] showed that, in the unobstructed in-plane network, the flows in G1B1 and G1B2 are identical, and the asymmetry in mass flow rate begins to grow from generation G2 onward. Figure 7 shows that the asymmetry exists in G1 itself when there is a blockage in G2B2 (which is downstream of generation G1). The asymmetry in mass flow rate increases with an increase in φ. This can be tied up with the corresponding changes in the velocity fields shown in Fig. 7. As an example, Fig. 7 shows that as the value of φ increases, the thickness of the boundary layer behaves differently on the two outer edges of the bifurcation connecting G0B1, G1B1 and G1B2: it increases on the outer edge that eventually merges with G1B1 but decreases on the outer edge that merges with G1B2. This disparity in the behaviour of the boundary layers is manifested in an increase in the asymmetry in the mass flow distribution between sub-networks L and R as compared to that in an unobstructed network.

Figure 8 shows how the velocity field at the end plane of a blocked branch (G2B2 in this example) changes as the extent of blockage changes. The primary velocity field is unidirectional in the unobstructed network ($\varphi = 0\%$) as well as in the presence of small blockage ($\varphi = 25\%$ in Fig. 8). Recirculation regions with oppositely directed velocity develop at larger values of φ (e.g. $\varphi = 50\%$ and $\varphi = 75\%$ in Fig. 8). As φ increases, the magnitude of the oppositely directed velocity and the extent of the recirculation region increase. The magnitude of the central jet-like velocity in the general direction G0 to G5 also increases as φ increases. The cross-sectional inhomogeneity of the velocity field thus increases with increasing φ. As a result of this, an apparently contradictory situation may arise in that, in the presence of blockage, the maximum velocity in a branch may increase while the mass flow rate through that branch decreases. Considerable changes in the vortical structure of the secondary motion also take place as φ increases. Figure 8 shows the existence of four vortices at $\varphi = 0\%$, two vortices at $\varphi = 25\%$ and no vortices at all at $\varphi = 50\%$ and $\varphi = 75\%$.

3.3 Effects of varying position of blockage

In order to determine the effect of position of the blockage in the network on the distribution of mass flow rate, nine cases are simulated: the unobstructed network and 75% blockage in eight different branches of sub-network L (one blockage at a time), viz. G2B1, G2B2, G3B1, G3B2, G3B3, G3B4, G4B5 and G4B6. Representative results for blockage in G2B1, G2B2, G3B3 and G3B4 are pictorially shown below. Similar

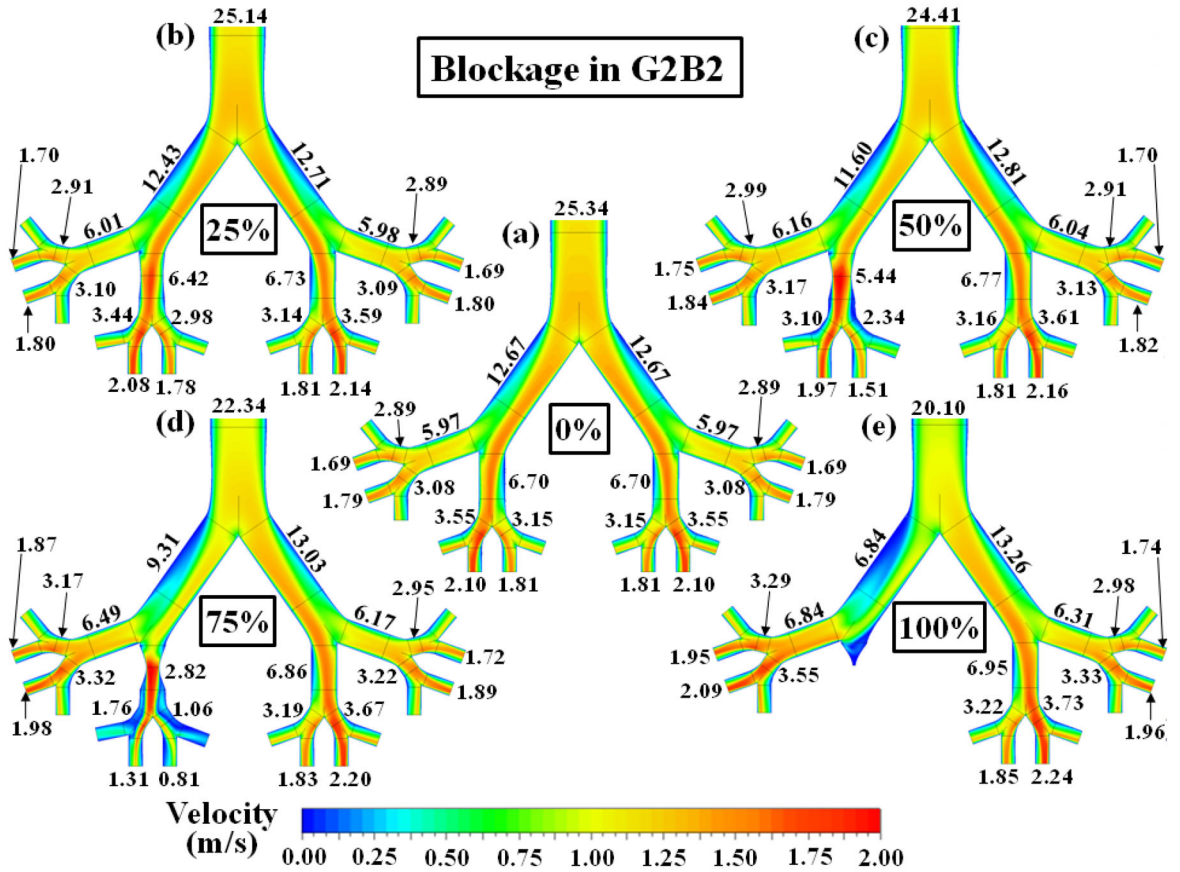

Fig. 7 Effect of varying extent of a blockage in G2B2 on the velocity field in the meridional plane and the overall mass flow distribution; in-plane configuration (Branches have been shown up to generation G4 for clarity, though the results reported are for the G0–G5 network. All mass flow rates are expressed in 10^{-5} kg/s)

diagrams for blockages in G3B1, G3B2, G4B5 and G4B6 were also constructed but not included here to save space.

Figure 9 shows the mass flow rates in the branches of a G0–G5 network for three cases, viz. when there is no blockage in the network, when there is a 75% blockage in branch G2B1 and when there is a 75% blockage in branch G2B2. The mass flow rate in the obstructed branch itself decreases by 55% and 60%, respectively, in the two cases of blockage. This is accompanied by an increase in mass flow rate in the sister of the obstructed branch—this increase in G2B2 is small for an obstruction in G2B1 while the increase is larger in G2B1 for an obstruction in G2B2 (in fact, the relative increase is maximum in G2B1 out of all branches in generation G2). The net effect of a significant decrease in the obstructed branch and a much smaller increase in the sister branch is a significant decrease in the mass flow rate in the mother branch (G1B1 in this case) and a significant decrease in the overall mass flow rate through the network. It is interesting to note that the total mass flow rate in the network remains almost unaltered by a shift of the blockage from G2B1 to G2B2. Figure 9 also shows that the mass flow rates in G1B2 and all the branches emanating from it (i.e. in sub-network R) are rather insensitive to a shift of the blockage from G2B1 to G2B2.

It is shown in Fig. 5 how the development of the jet-like stream along the centreline of the blocked branch (G2B2) leads to highly skewed velocity profiles in its daughter branches (G3B3 and G3B4), which, on division, creates further flow non-uniformity among its granddaughter branches (G4B5–G4B8). Such non-uniformity in the velocity field is connected to the non-uniform distribution in mass flow rates among the concerned branches. This principle is exemplified in Fig. 9, which shows that blockage in G2B1 results in the generation of a high degree of non-uniformity in the mass flow distribution among branches G4B1–G4B4 with the mass flow rates in G4B2 and G4B3 (which are aligned with G2B1) being approximately 3 times (for $\varphi = 75\%$) that in G4B1 and G4B4 (i.e. branches that are not aligned with G2B1). This factor is about 1.5 in an unobstructed network.

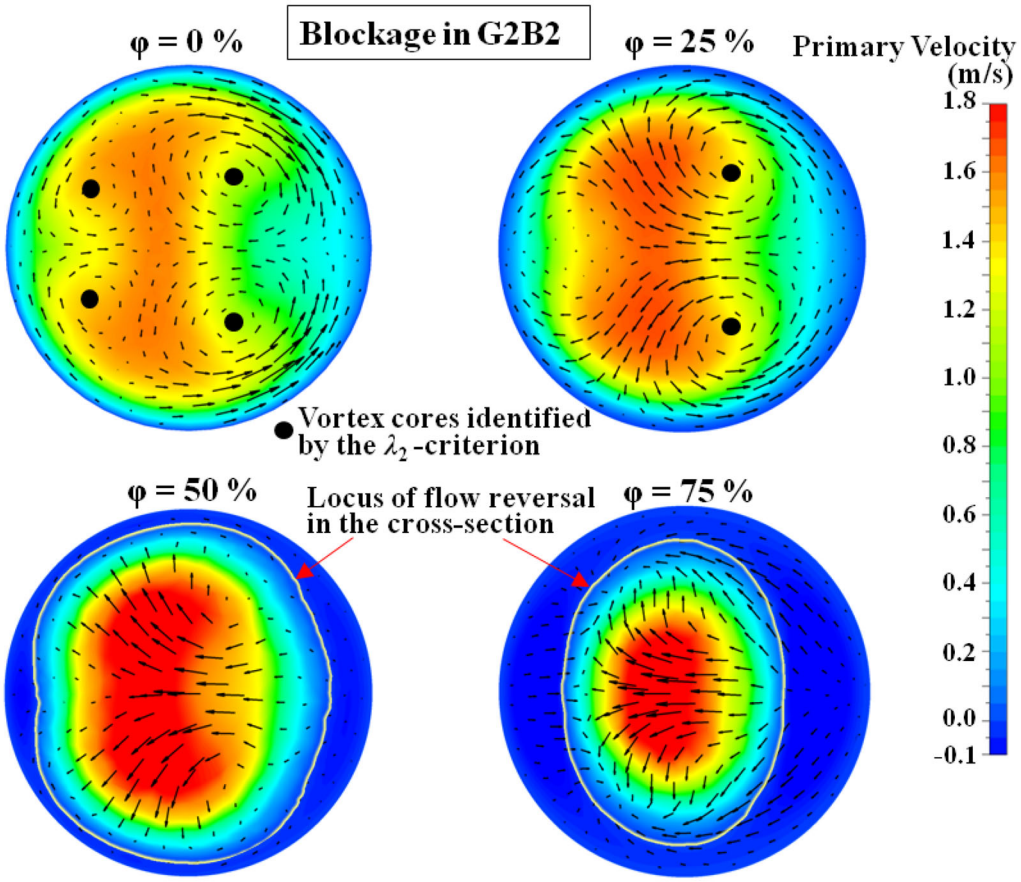

Fig. 8 Primary velocity contours with superposed secondary velocity vectors at the end plane of G2B2 downstream of the blockage for various values of the extent of blockage (φ); in-plane configuration (The closed curves are constructed through post-processing to clearly demarcate two regions with opposite directions of primary flow)

Figure 10 shows the effects of a blockage in generation G3 on the mass flow distribution in the network. A blockage in generation G3 produces similar general trends in terms of the decrease in mass flow rate in the obstructed branch, of the increase or decrease in mass flow rates in the remaining branches of the network and of the alteration in mass flow asymmetry as discussed previously in connection with a blockage in generation G2. It is also found in Figs. 9 and 10 that the maximum relative increase in the mass flow rate usually occurs in the sister branch of the obstructed branch. This principle may, however, be violated if the sister of the obstructed branch falls in the maximum flow path (e.g. G0B1–G5B11 in this configuration) of the unobstructed network.

Table 4 shows the effects of a blockage in G4B5 or G4B6 on the mass flow rates along all flow paths, from the main inlet to the outlets of the computational domain, which contain their grandmother branch G2B2. (Quantitative results are presented for only these branches to save space, noting that the mass flow rates in all the other branches of the network are only slightly affected.) A comparison of the mass flow rate in G0B1 in Figs. 9, 10 and Table 4 shows that the decrease in the overall mass flow rate (with respect to the unobstructed network) is smaller as the blockage shifts to downstream generations. Though the effect of a blockage of fixed magnitude seems to decrease as it shifts downstream, it should be noted that the change in diameter between the unobstructed branch and the throat of the blockage ($d_{\text{branch}} - d_{\text{throat}}$) required to achieve the same value of φ also decreases down the generations due to a decrease in d_{branch}. In the biological context, the same thickness of plaque formation on the branch wall would thus lead to greater values of φ in downstream branches.

4 Reflections on the flow solutions obtained by using 3D computation and 1D model

This section is introduced to assess what qualitative and quantitative information regarding the flow through unobstructed or obstructed branching networks can be captured by a simpler one-dimensional (1D) mathe-

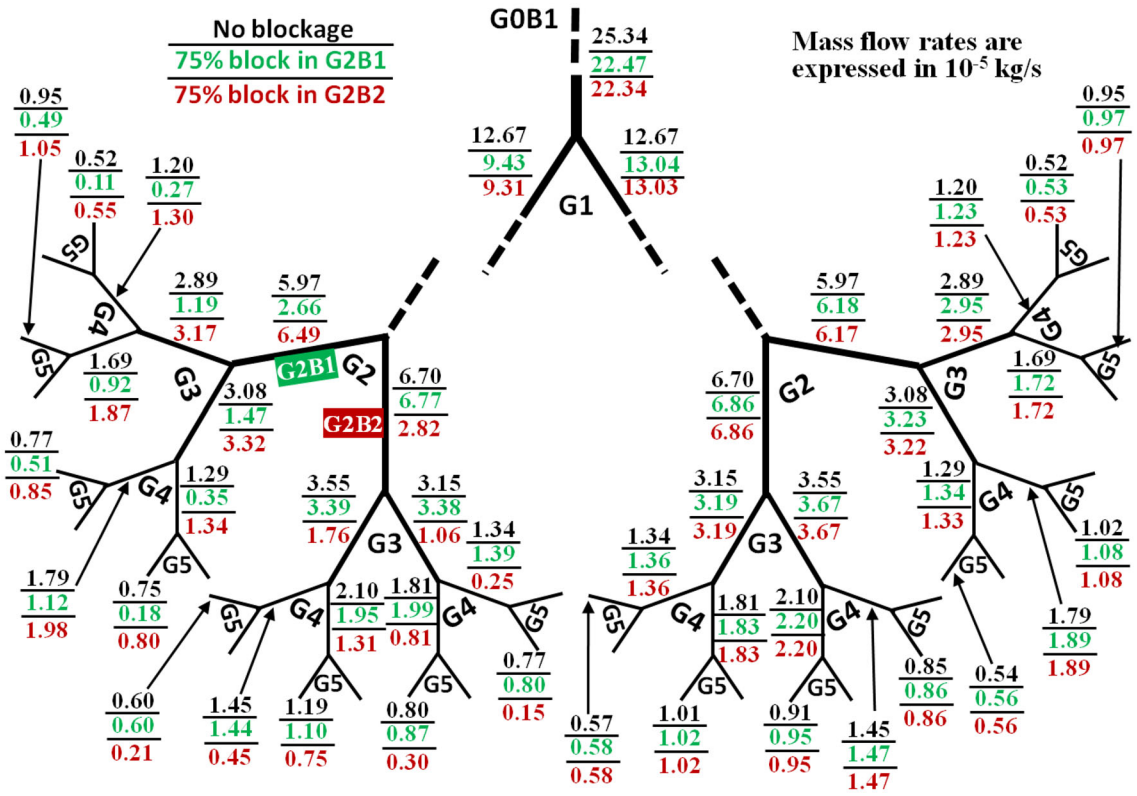

Fig. 9 A comparison of the mass flow distribution in the branches of a G0–G5 network without any blockage with that when a blockage ($\varphi = 75\%$) is present in branch G2B1 or G2B2 for $p_{\text{total,in}} = 2.7$ Pa; in-plane configuration

matical model based on the Hagen–Poiseuille formulation for pressure drop. Details of the calculation method for the 1D models for both unobstructed and obstructed flows, and a comparison of the mass flow rates in the unobstructed G0–G5 network obtained from the 1D model and 3D computations is given in the "Appendix". Sample results for obstructed flow, with a 75% blockage in G2B2, are presented in Fig. 11.

As in the case of the unobstructed network ("Appendix"), the mass flow rate entering the network in this case also is overestimated by the 1D model. Although the qualitative features such as the reduction of the mass flow rate in the obstructed branch (G2B2) and an increase in the same in its sister branch (G2B1) are also present in the predictions of the 1D model, the quantitative information is not accurate. Moreover, the 1D model predicts that the flow would subsequently be equally divided in the branches downstream of G2B2. Thus, although the 1D model predictions show some non-uniformity in the distribution of mass flow rates, it is unable to capture the highly non-uniform mass flow distribution in granddaughters of the obstructed branch. For the example shown in Fig. 11, the 1D model calculations show only three different mass flow rates in the branches of a generation from G2 onward (i.e. G2, G3, G4, G5), the mass flow rates in the branches of the same generation determined by 3D computation are all different.

The methodology for 1D loss calculation given in the "Appendix" may be improved by including the loss incurred in the bifurcation module itself [11]. We are working towards the development of a generic formulation for this. The task is formidable, and even if the goal is achieved, it is important to realize that the thus improved 1D model would still not be capable of predicting different flow solutions in the various branches of any generation of a geometrically symmetric network.

The 1D model misses the three-dimensional alteration to the flow field that is caused by the presence of a blockage. Because of the predicted flow symmetry among the branches of any generation in the unobstructed network, the 1D model gives equivalent flow structure in an obstructed network if a blockage of fixed magnitude is shifted between various branches of a particular generation (while the 3D computations produce fundamentally different solutions if a blockage is shifted likewise in the sub-network L). Moreover, a 1D model cannot differentiate between the in-plane and out-of-plane configurations and hence it is not possible to assess the dependence of flow alteration due to blockage on the three-dimensional arrangement of branches

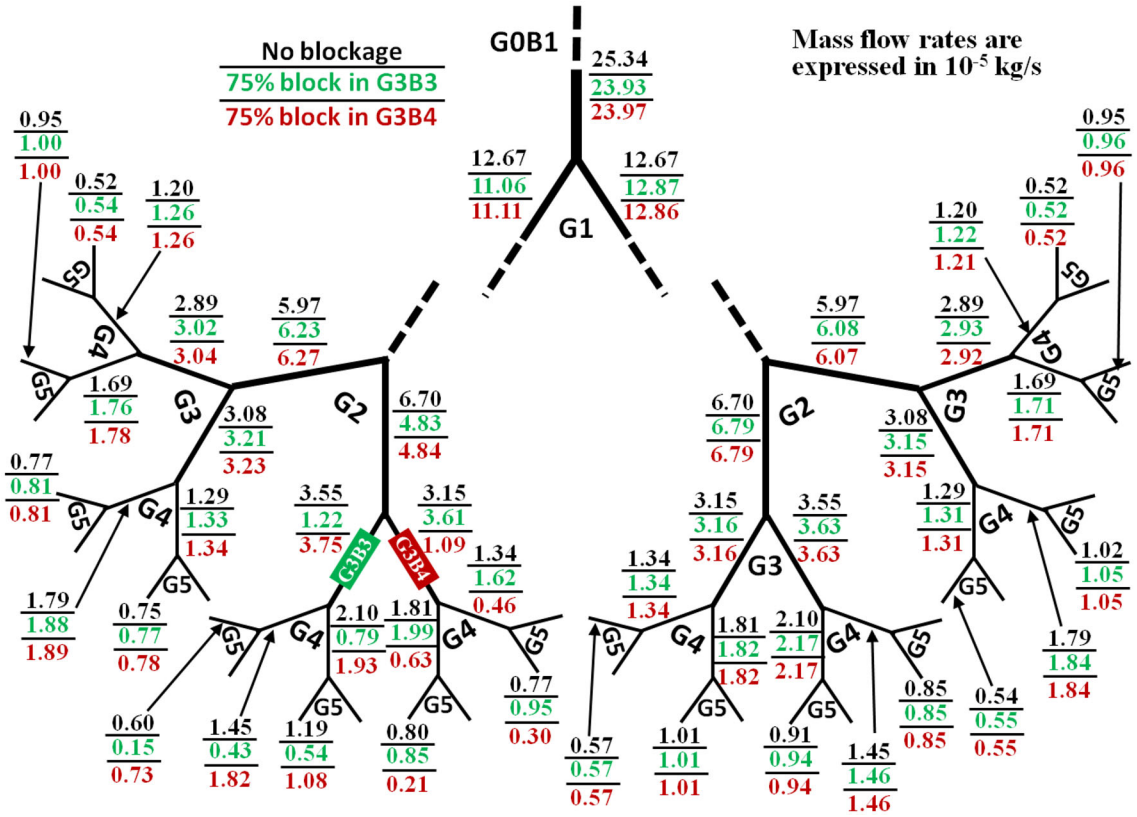

Fig. 10 A comparison of the mass flow distribution in the branches of a G0–G5 network without any blockage with that when a blockage ($\varphi = 75\%$) is present in branch G3B3 or G3B4 for $p_{\text{total,in}} = 2.7$ Pa; in-plane configuration

Table 4 Mass flow rates in selected branches of the in-plane G0–G5 network without any blockage and when a blockage ($\varphi = 75\%$) is present in a branch of generation G4 for $p_{\text{total,in}} = 2.7$ Pa

	G0B1	G1B1	G2B2	G3B3	G3B4	G4B5	G4B6	G4B7	G4B8
Unobstructed network	25.34	12.67	6.70	3.55	3.15	1.45	2.10	1.81	1.34
75% blockage in G4B5	24.89	12.15	6.09	2.72	3.37	0.55	2.17	1.90	1.47
75% blockage in G4B6	24.87	12.13	6.07	2.69	3.38	1.94	0.75	1.90	1.48
	G5B9	G5B10	G5B11	G5B12	G5B13	G5B14	G5B15	G5B16	
Unobstructed network	0.60	0.85	1.19	0.91	0.80	1.01	0.77	0.67	
75% blockage in G4B5	0.20	0.35	1.14	1.03	0.83	1.07	0.84	0.63	
75% blockage in G4B6	0.86	1.08	0.43	0.32	0.83	1.07	0.85	0.63	

Mass flow rates are expressed in 10^{-5} kg/s

by using the 1D model. (The out-of-plane configuration is, however, a more realistic situation in the biological context.) It is quite evident from the above discussion that the 1D model is unable to capture the qualitative characteristics or the quantitative details of the flow in branching networks in the presence of a blockage or in its absence ("Appendix"). This renders the 3D computations necessary.

5 Results and discussion for the out-of-plane configuration

It is explained in Sect. 2 that it is necessary and sufficient to determine the effects of a blockage in branches lying in a quarter of the network (denoted as sub-networks L1, L2, R1 and R2 in Sect. 2) for the out-of-plane configuration, though for a particular blockage the flow field in the entire network needs to be simulated. Accordingly, here we consider the effects of blockage in branches lying in one of the four above-mentioned

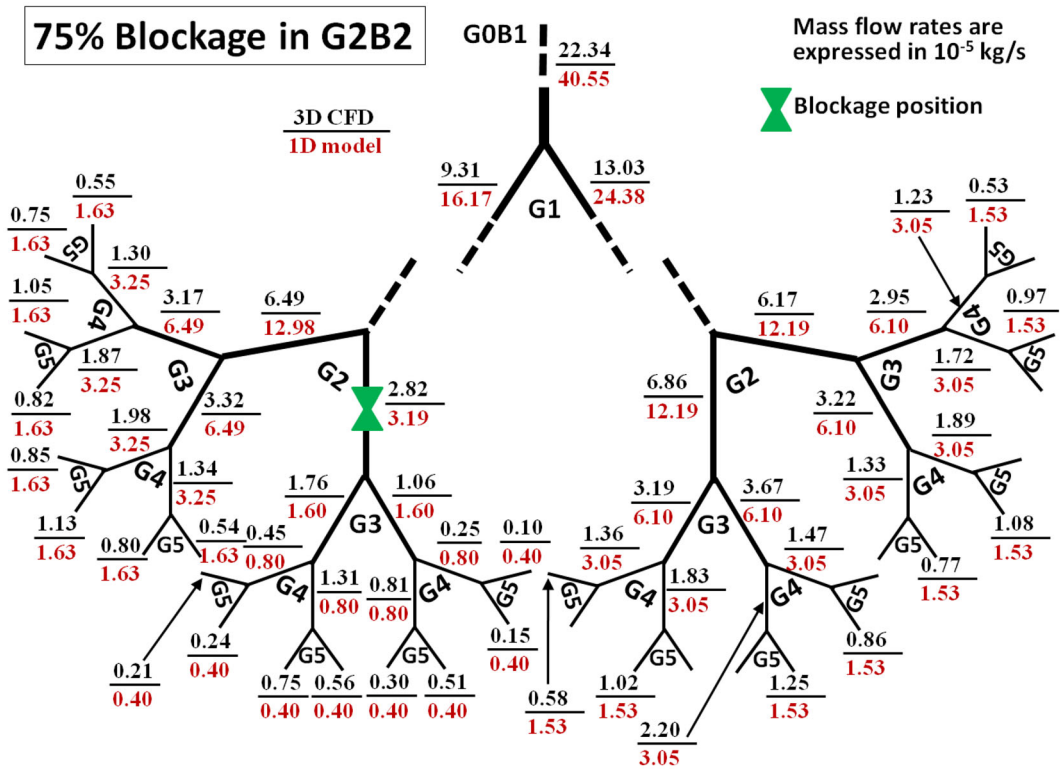

Fig. 11 A comparison of the mass flow distribution in the G0–G5 network with an obstruction in G2B2, obtained from the 3D computations with those predicted by a 1D model for the same pressure drop across the network

sub-networks. An initial CFD simulation, using inlet velocity condition, determined that an inlet Reynolds number of 1000 requires $p_{\text{total,in}} = 2.738$ Pa in unobstructed out-of-plane G0–G5 network. This total pressure at inlet is specified in the simulations described in this section so as to keep the driving potential constant for all cases of blockage.

5.1 General effects of blockage on flow field

It is found that as in the case of the in-plane configuration, a blockage in a branch in the out-of-plane configuration also results in a reduction in the mass flow rate through it. Figure 12 shows the evolution of the flow field downstream of a 75% blockage in G2B1, revealing the important differences between the effects of a blockage in a large out-of-plane network and that in its in-plane counterpart. (i) It is shown in Ref. [4] that even for an unobstructed network, the difference in the flow fields among the branches of a generation is considerably smaller for the out-of-plane configuration than that in the in-plane configuration. A comparison of Figs. 5 and 12 shows that this trend is retained in both generations G3 and G4 even in the presence of a blockage in G2. In spite of the increased inhomogeneity in the cross-sectional velocity distribution due to the formation of the central jet-like stream downstream of a blockage in the out-of-plane configuration, the rotation of successive flow units through 90° results in smaller differences in the flow fields in the downstream branches. (ii) While the recirculation regions were found to persist even up to generation G4 (Fig. 5) for a blockage in a branch of generation G2 in the in-plane configuration, Fig. 12 shows that for a 75% blockage in G2B1 in the out-of-plane configuration, recirculation regions persist up to G3 only. Therefore, the three-dimensional arrangement of the branches affects the reattachment lengths. Although not evident in Fig. 12, the general trend of different reattachment lengths along different flow paths (Fig. 5) is found to hold good for this configuration as well.

It is shown in Ref. [4] that, in an unobstructed network, the asymmetry in the mass flow distributions between various branches of a generation for the out-of-plane configuration can be an order of magnitude smaller than that in in-plane configuration. From the comparative study of Figs. 5 and 12, it might seem that this order of magnitude difference could be maintained between the two configurations even in the presence of

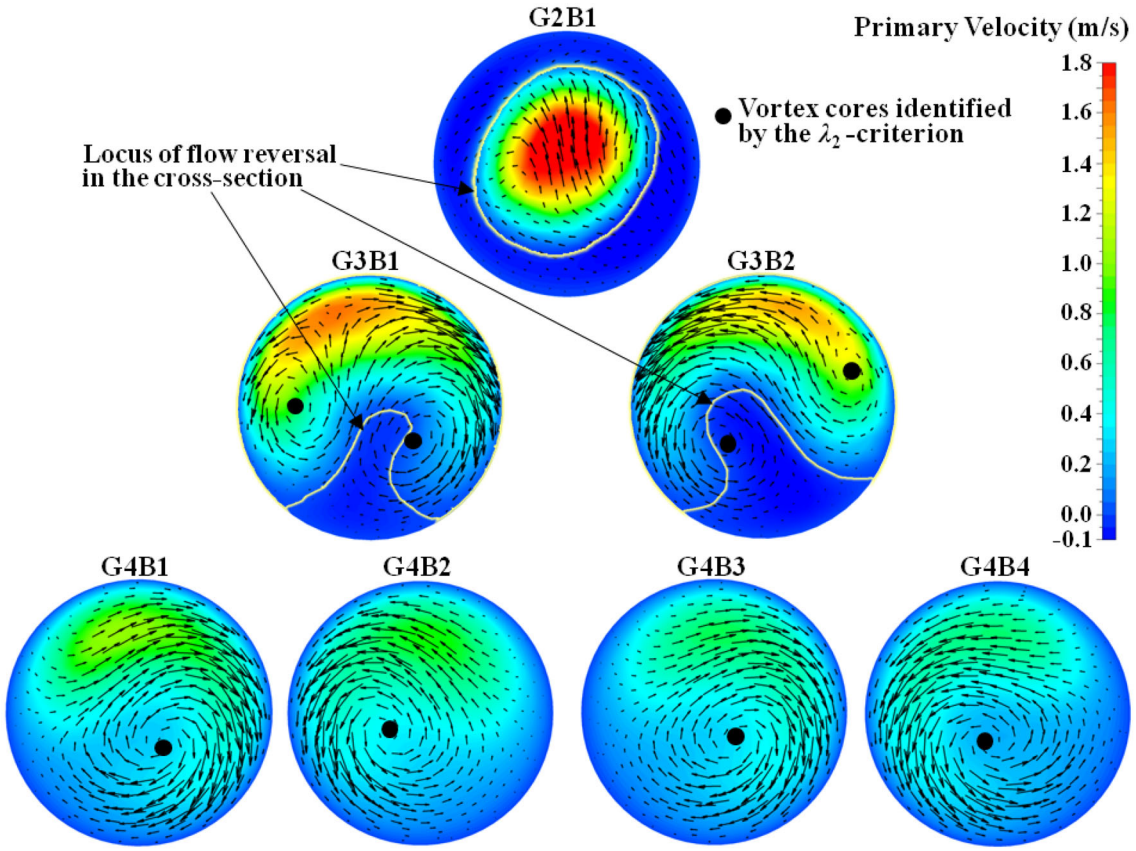

Fig. 12 Contours of primary velocity with superposed secondary velocity vectors at end- planes of the named branches for 75% blockage in G2B1; out-of-plane configuration (The adopted representational convention is such that the downstream bifurcation ridge appears as a vertical line in the diagram and the primary flow is towards the reader)

a blockage. However, it is to be remembered that the difference between the maximum and minimum mass flow rates in a generation increases considerably due to the decrease in the mass flow rate in the blocked branch and its downstream branches, and the simultaneous increase (small or large) in the mass flow rates in the remaining branches. This leads to a significant increase in the asymmetry of mass flow rates in the presence of a blockage in the out-of-plane configuration, the increase being comparable to that in in-plane configuration.

It is shown in Ref. [5] that in the unobstructed out-of-plane network, there are three vortices in G2B1, two vortices in all branches of G3 and in three of the four branches of G4 in sub-network L1 (while part length of one branch contains three vortices, though only two vortices are seen at the end plane of this branch also). Figure 12 shows that the presence of a large (75%) blockage removes any vortical pattern at the end plane of the blocked branch (G2B1). However, a two-vortex system is re-established in G3B1 and G3B2, the location of the vortices being different from that in the unobstructed network. Figure 12 shows that one vortex occurs on the end plane of the G4 branches (instead of two vortices in the unobstructed network). The presence of blockage therefore significantly alters the secondary flow patterns in the downstream branches.

Figure 13 shows the effects of a 75% blockage in G2B2 on the distribution of the magnitude of secondary flow at the start planes of the blocked branch and its downstream branches for the out-of-plane configuration. It was shown in Ref. [5] that, in contrast to the velocity field in the in-plane configuration, there exists no plane of symmetry in the flow field in branches of the out-of-plane configuration from generation G2 onwards. This holds true in the presence of a blockage as well. While the reduction of secondary velocity in the blocked branch and increase in inhomogeneity in the cross-sectional secondary velocity distribution in its downstream branches are similar to the effects of a blockage in the in-plane configuration, there exist differences between the effects of a blockage in the two configurations. A comparison of the corresponding diagrams in Fig. 13a, b shows that the blockage in G2B2, in the out-of-plane configuration, decreases the differences in the secondary velocity distribution among the granddaughters; the contours of $|\vec{v}_S|$ at G4B5 and G4B8, and those at G4B6

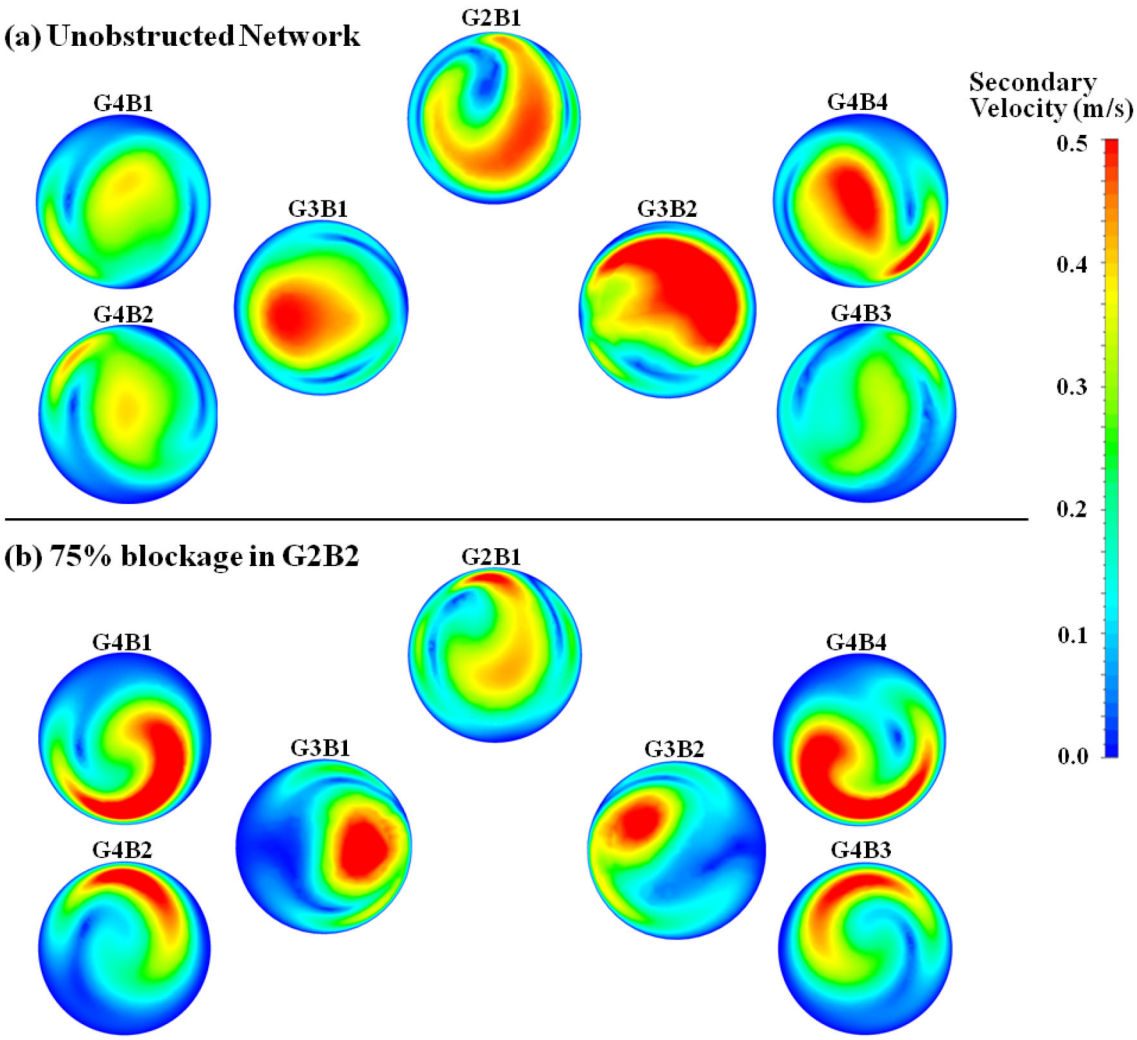

Fig. 13 Effect of blockage on the magnitude of secondary flow at the start planes of the blocked branch and its downstream branches; out-of-plane configuration

and G4B7 turn out to be similar to each other in the presence of a blockage. Figure 6 shows that the presence of a blockage accentuates the differences in corresponding secondary flows in the in-plane configuration.

5.2 Effects of the extent of blockage on velocity and mass distributions

Three cases corresponding to $\varphi = 0\%$, $\varphi = 50\%$ and $\varphi = 100\%$ for a blockage in G2B1 in the out-of-plane configuration are considered. It is found that an increase in φ in the out-of-plane configuration has the same effects on the pressure drop across the network and overall mass flow rate in the network as that found in Table 3 for the in-plane configuration.

Figure 14 shows the velocity distribution on the local meridional planes of successive flow units (comprising a mother branch, its two daughter branches and the connecting bifurcation module) and the mass flow rates up to generation G4 of the G0–G5 network. Since any two successive flow units in the out-of-plane configuration are perpendicular to each other, their local meridional planes also lie at right angle to each other. This feature is represented in Fig. 14 by the discontinuities between successive flow units. It is found that a blockage in G2B1 results in a reduction in the mass flow rate through that branch and a much smaller increase in the mass flow rate through G2B2. Consequently, the overall mass flow rate in the network decreases, this decrease being enhanced by an increase in φ. As the extent of blockage is increased, the changes (with respect to unobstructed

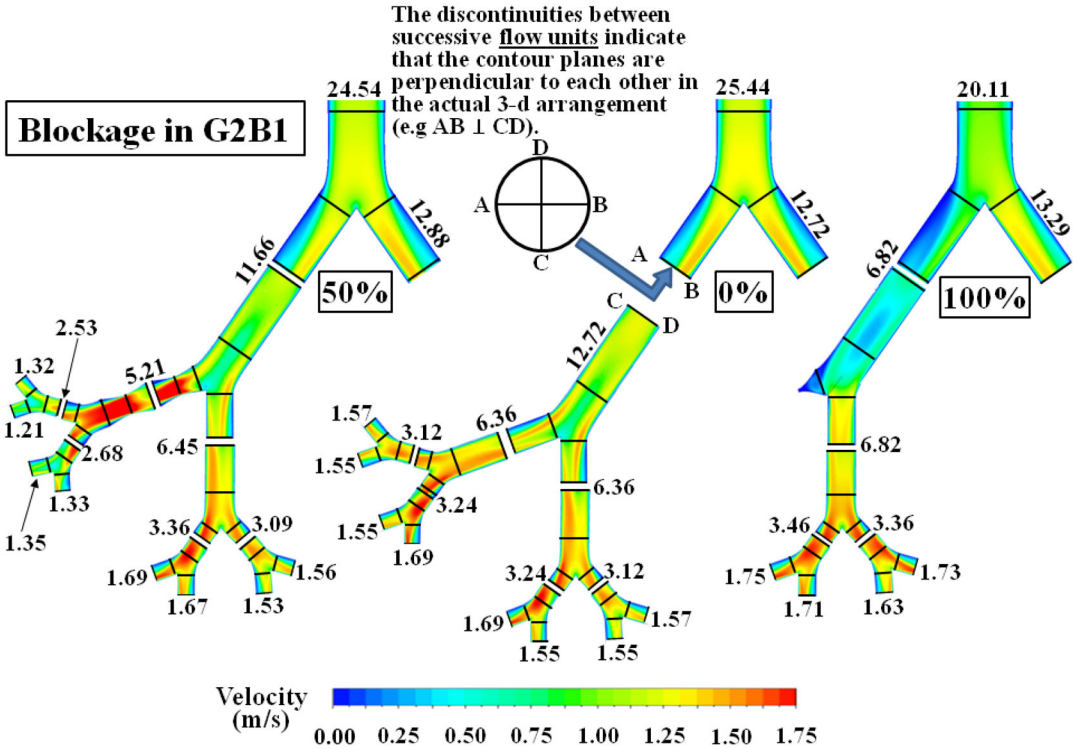

Fig. 14 Effect of varying extent of a blockage in G2B1 on the velocity field in the local meridional planes of successive flow units and the overall mass flow distribution; out-of-plane configuration (Branches have been shown up to generation G4 for clarity, though the results reported are for the G0–G5 network. All mass flow rates are expressed in 10^{-5} kg/s)

network) in mass flow rates through all branches increase; the same additional change in φ having greater effect as the value of φ itself increases.

Ref. [4] showed that, in the unobstructed out-of-plane network, the flows in the four G2 branches are identical, and the asymmetry in mass flow rate begins to grow from generation G3 onward. Figure 14 shows that the asymmetry exists in G1 itself when there is a blockage in G2B1 (which is downstream of generation G1). A comparison of Figs. 7 and 14 shows that for a given nonzero value of φ, the level of asymmetry developed in the mass flow rates in generation G1 for the out-of-plane configuration is similar to that in its in-plane counterpart. The asymmetry in mass flow rates among the branches of a generation increases with an increase in φ. Similar to the finding in Fig. 7 for the in-plane configuration, it was found (not shown here) that the mass flow distribution in sub-network R of the out-of-plane configuration remains qualitatively unaltered due to a blockage in sub-network L. However, a blockage in sub-network L1 does qualitatively affect the mass flow distribution in sub-network L2. As an example, a 50% blockage in G2B1 results in a 4% increase in the mass flow rate in G3B3 but a 1% decrease in the same in G3B4.

Figure 15 shows how the velocity field at the end plane of a blocked branch (G2B1 in this example) changes as the extent of blockage changes. As for the in-plane configuration (Fig. 8), the primary velocity field in the out-of-plane configuration (Fig. 15) is found to be unidirectional in the unobstructed network as well as in the presence of small blockage ($\varphi = 25\%$ in Fig. 15), with recirculation regions and bi-directional flow developing at larger values of φ (e.g. $\varphi = 50\%$ and $\varphi = 75\%$). Moreover, other features identified in Fig. 8 such as increased magnitude of oppositely directed flow, increased magnitude of the jet velocity, increased extent of the recirculation region and consequent increase in cross-sectional inhomogeneity of the velocity field with increasing φ are found to hold good in the out-of-plane configuration as well (Fig. 15). Considerable differences exist in the changes in the vortical structure of the secondary motion that take place with increasing φ in the two configurations. While Fig. 8 shows a change from a four-vortex system at $\varphi = 0\%$ to a two-vortex system at $\varphi = 25\%$ to a pattern free of any vortices at $\varphi = 50\%$ and $\varphi = 75\%$, Fig. 15 shows the existence of three vortices at $\varphi = 0\%$ and $\varphi = 25\%$, a single vortex at $\varphi = 50\%$ and no vortices at all at $\varphi = 75\%$.

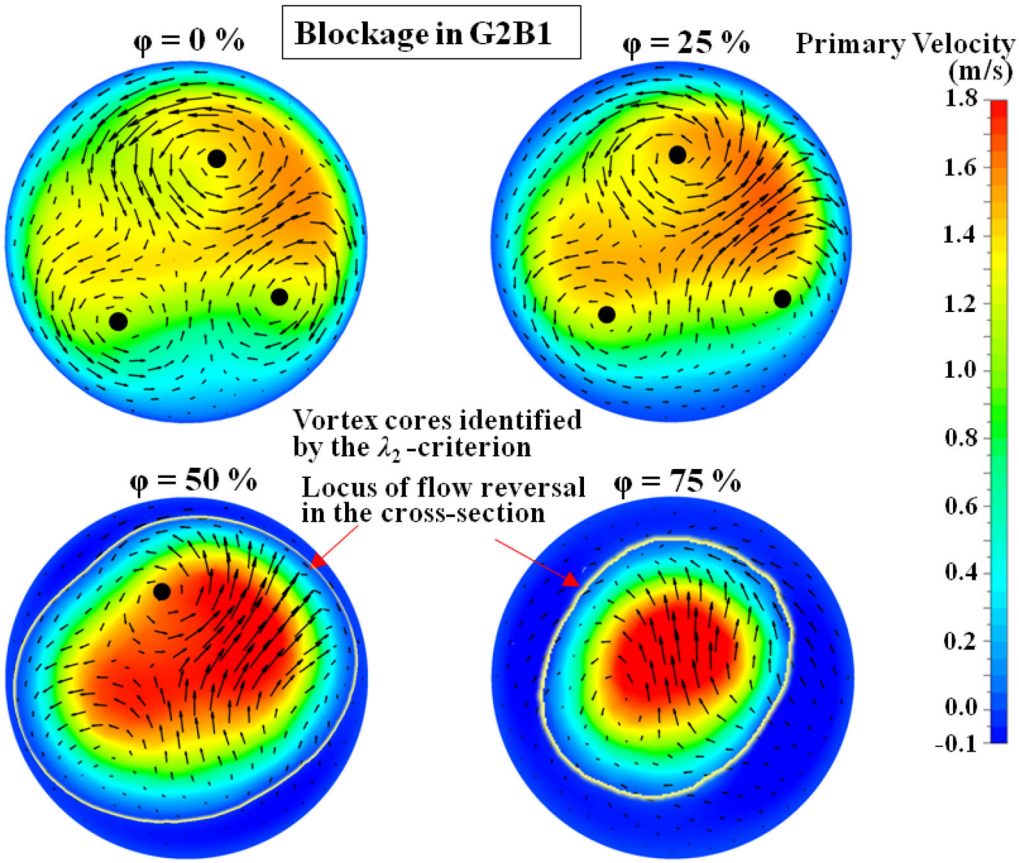

Fig. 15 Primary velocity contours with superposed secondary velocity vectors at the end plane of G2B1 downstream of the blockage for various values of the extent of blockage (φ); out-of-plane configuration (The closed curves are constructed through post-processing to clearly demarcate two regions with opposite directions of primary flow)

5.3 Effects of varying position of blockage

In order to determine the effect of position of blockage in the network on the distribution of mass flow rate, eight cases are simulated: the unobstructed network and 75% blockage in seven different branches of sub-network L1 (Sect. 2), with one blockage at a time in G2B1, G3B1, G3B2, G4B1, G4B2, G4B3 and G4B4. Representative results for blockage in G2B1, G3B1, G3B2 and G4B3 are pictorially shown here.

Figure 16 shows that a large blockage in G2B1 causes a large reduction in mass flow rate through G2B1, a small increase in G2B2 and thus a significant reduction in the overall mass flow rate (G0B1). The blockage in G2B1 is found to have a strong impact on the mass flow rates in all downstream branches originating from G2B1. However, unlike in the in-plane configuration, the non-uniformity in the distribution of mass flow rates in these branches is only slightly affected. This may be attributed to the three-dimensional arrangement of the branches in the 90° out-of-plane configuration which results in a lower cumulative asymmetry [4] in the mass flow distribution as the fluid travels down the generations.

It is interesting to note that while the mass flow rate in G3B1 is smaller than that in G3B2 in the unobstructed network, a blockage in G2B1 reverses this distribution (i.e. mass flow rate in G3B1 becomes greater than that in G3B2). A change in the cross-sectional asymmetry in velocity distribution in G2B1 about its downstream bifurcation ridge, shown in Fig. 17, is the reason for the aforementioned reversal (which was not seen in in-plane configuration). This is an evidence that even a geometrically symmetric blockage can cause asymmetric three-dimensional alteration to the velocity field (primary and secondary). The aforementioned reversal also happens in branches G4B3 and G4B4 for a 75% blockage in G3B2 (Fig. 18). The reversal, however, does not happen for a similar level of blockage in G3B1.

Table 5 shows the effects of a blockage in G4B3 or G4B4 on the mass flow rates along all flow paths, from the main inlet to the outlets of the computational domain, which contain their grandmother branch G2B1.

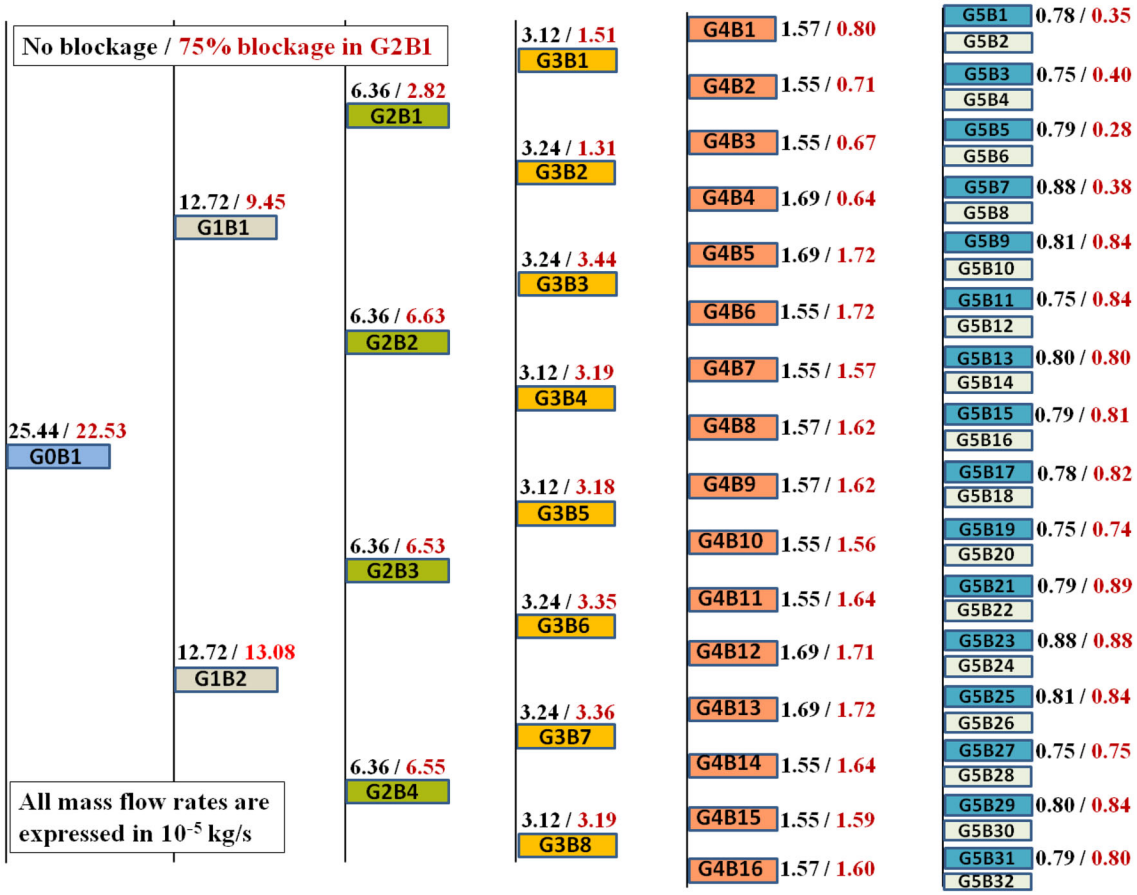

Fig. 16 A comparison of the mass flow rate distribution in all branches of a G0–G5 network without any blockage with that when a blockage ($\varphi = 75\%$) is present in branch G2B1 for $p_{\text{total,in}} = 2.738$ Pa; out-of-plane configuration

(Quantitative results are presented for only these branches to save space, noting that the mass flow rates in all the other branches of the network are only slightly affected.) A reversal of which of the two sister branches G5B5 and G5B6 receives greater mass flow rate happens for a 75% blockage in G4B3 with an extreme example of asymmetry: G5B5 and G5B6 receive, respectively, 0.79×10^{-5} kg/s and 0.76×10^{-5} kg/s in unobstructed flow, but they receive, respectively, 0.08×10^{-5} kg/s and 0.43×10^{-5} kg/s for a 75% blockage in G4B3. The fluid dynamics is explained in Fig. 19, which shows that the presence of high level of cross-sectional flow asymmetry (at plane G4S3) *upstream* of the blockage is responsible for the observed highly asymmetric three-dimensional modification to the flow field caused by the blockage (even though the blockage geometry is chosen to be symmetric in the example calculations).

6 A synthesis of the effects of blockage in a network

6.1 Common features in in-plane and out-of-plane network

A few general features of the effects of blockage on the flow in a network, either in-plane or out-of-plane, can be deduced from the computations described in Sects. 3 and 5: (i) The presence of a blockage in a branch always results in a reduction in the mass flow rate through that branch, its daughter and granddaughter branches in subsequent generations and in all upstream branches that fall along the flow path between the main inlet and the obstructed branch. (ii) The presence of a blockage results in an increase in the mass flow rate through its sister branch. (iii) The presence of a blockage results in a decrease in the total mass flow rate at the inlet of the network, the magnitude of this decrease being reduced as the position of the blockage shifts downstream. and a decrease in the mass flow rate at the inlet to the network. (iv) When a blockage is shifted from one branch

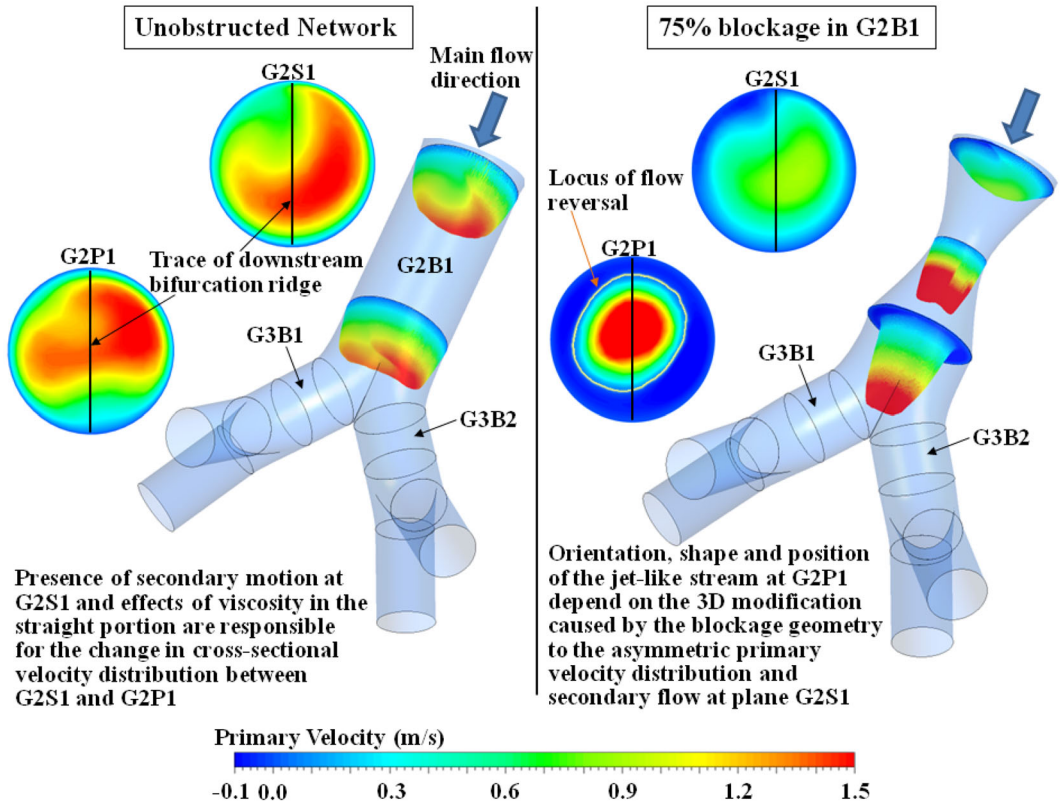

Fig. 17 Which of the two sister branches G3B1 and G3B2 would receive greater mass flow rate changes due to a 75% blockage in G2B1; fluid dynamics in out-of-plane configuration (Velocity distribution about downstream bifurcation ridge indicates the mass flow distribution among the daughter branches. 3D representation is formed by the envelope of velocity vectors drawn on each selected cross-sectional plane. The lengths of velocity vectors indicate magnitude which is also colour-coded)

to its sister, it is found that the mass flow rates are significantly altered in only these two branches and all branches that emanate from them. (v) When a blockage of a fixed magnitude is shifted from one branch to any other branch of a given generation G*n*, the overall mass flow rate at the inlet of the network is found to remain nearly unaltered.

6.2 Influence of the branching configurations on the effects of blockage

While presenting the general features of obstructed flow in out-of-plane configuration, a comparative analysis of the two configurations is included wherever possible in Sect. 5. This discussion on the dependence of the effects of a blockage on the three-dimensional arrangement of the same individual branches is consolidated here through representation of three-dimensional velocity field and further analysis of complementary issues.

Figures 20 and 21 show the effects of a 75% blockage in G2B2 on the three-dimensional evolution of the velocity field in the blocked branch and in its downstream branches for the in-plane and out-of-plane configurations, respectively. (The branches of generation G5 are not shown in Fig. 21 since they obstruct the view and make it difficult to show the velocity distributions in the branches of generations G3 and G4.) The significantly reduced velocity at the start plane of the blocked branch as compared to the unobstructed branch shows that, along with downstream branches, the blockage affects the upstream flow field considerably. Since no recirculatory flow is observed during inspiration in the adopted geometry of the unobstructed network, it can be concluded that the recirculation regions found in Figs. 20b and 21b are caused solely by the presence of blockage. The recirculation region extends to different lengths along different flow paths. The central jet-like stream in the blocked branch G2B2 leads to an increased asymmetry (about their upstream bifurcation ridge) in the cross-sectional velocity distribution in G3B3 and G3B4 with the maximum flow shifted towards the inner edge of the preceding bifurcation. However, the rotation of successive flow units through 90° in the out-of-

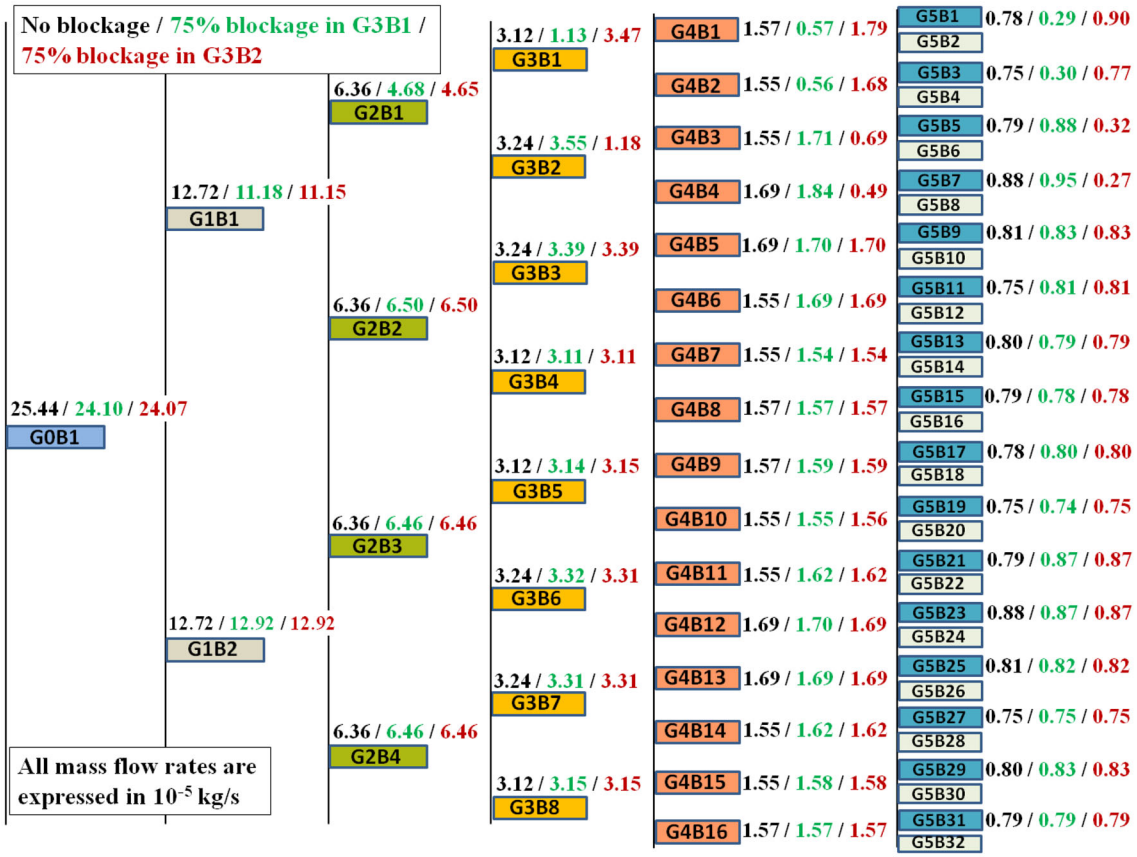

Fig. 18 A comparison of the mass flow rate distribution in all branches of a G0–G5 network without any blockage with that when a blockage ($\varphi = 75\%$) is present in branch G3B1 or G3B2 for $p_{\text{total,in}} = 2.738$ Pa; out-of-plane configuration

Table 5 Mass flow rates in selected branches of the out-of-plane G0–G5 network without any blockage and when a blockage ($\varphi = 75\%$) is present in a branch of generation G4 for $p_{\text{total,in}} = 2.738$ Pa; out-of-plane configuration

	G0B1	G1B1	G2B1	G3B1	G3B2	G4B1	G4B2	G4B3	G4B4
Unobstructed network	25.44	12.72	6.36	3.12	3.24	1.57	1.55	1.55	1.69
75% blockage in G4B3	24.89	12.06	5.64	3.29	2.35	1.67	1.62	0.51	1.84
75% blockage in G4B4	24.87	12.03	5.60	3.30	2.30	1.68	1.62	1.77	0.53
	G5B1	G5B2	G5B3	G5B4	G5B5	G5B6	G5B7	G5B8	
Unobstructed network	0.78	0.79	0.75	0.80	0.79	0.76	0.88	0.81	
75% blockage in G4B3	0.84	0.83	0.76	0.86	0.08	0.43	0.99	0.85	
75% blockage in G4B4	0.85	0.83	0.76	0.86	0.89	0.88	0.51	0.02	

Mass flow rates are expressed in 10^{-5} kg/s

plane configuration ensures that the asymmetry is not enhanced about their respective downstream bifurcation ridges as significantly as it does in the in-plane configuration. Therefore, the difference between the velocity distributions among the G4 branches downstream of G2B2 is much smaller than that observed for the in-plane configuration.

A new concept called 'degree of mass flow asymmetry' ($\delta_{\text{G}n}$) was introduced in Ref. [4] which gives a quantitative measure of the non-uniformity in the mass flow rates in various branches of a particular generation. It is defined as follows:

$$\delta_{\text{G}n} \equiv (\dot{m}_{\text{G}n,\max} - \dot{m}_{\text{G}n,\min}) \big/ \dot{m}_{\text{G}n,\text{avg}} \tag{4}$$

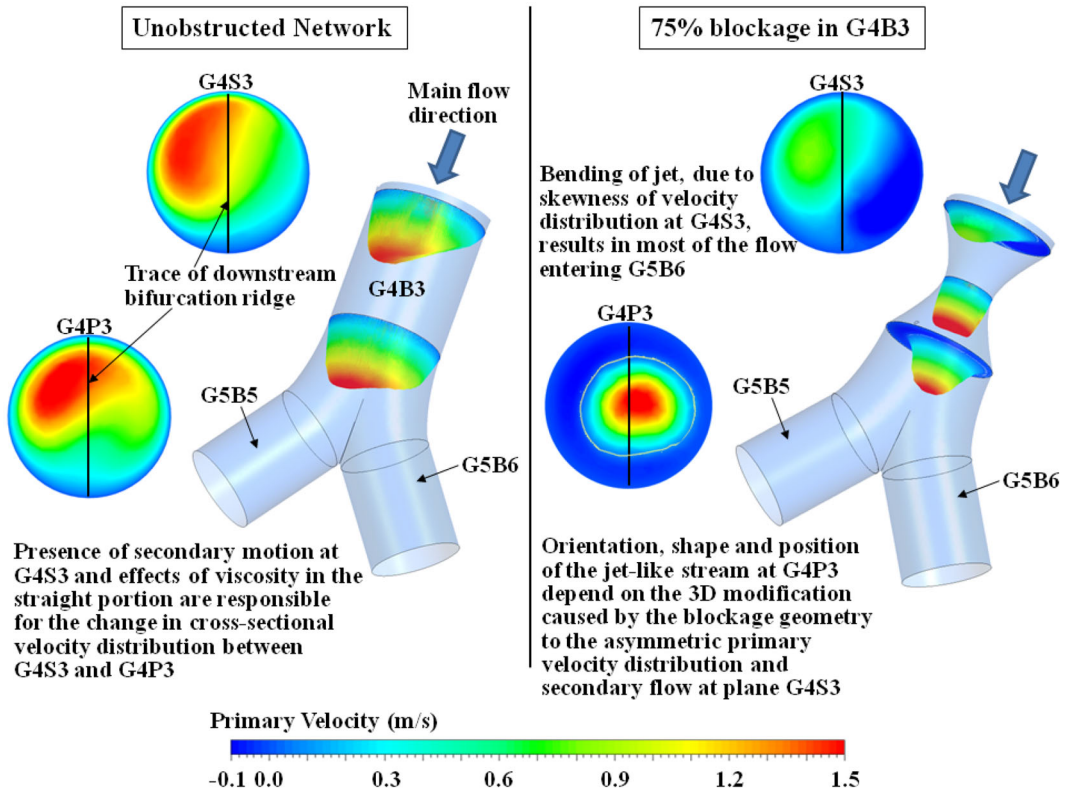

Fig. 19 Fluid dynamic reasons for the reversal of which of the two sister branches G5B5 and G5B6 receives greater mass flow rate, and an extreme increase in the mass flow asymmetry between the two branches, due to a 75% blockage in G4B3; out-of-plane configuration (Velocity distribution about downstream bifurcation ridge indicates the mass flow distribution among the daughter branches. 3D representation is formed by the envelope of velocity vectors drawn on each selected cross-sectional plane. The lengths of velocity vectors indicate magnitude which is also colour-coded)

where, $\dot{m}_{Gn,\text{avg}}$ ($\equiv \frac{1}{2^n}\sum_{k=1}^{k=2^n} \dot{m}_{Gn,k}$) is the average mass flow rate per branch in generation Gn, and, $\dot{m}_{Gn,\max}$ and $\dot{m}_{Gn,\min}$ are the maximum and minimum flow rates in that generation. Figure 22 shows the variation of δ_{Gn} in the successive generations of the G0–G5 network for various blockage locations for both configurations.

The following general observations can be made regarding the variation of δ_{Gn} in the unobstructed network. δ_{Gn} grows in each successive generation, starting from G2 for the in-plane configuration and from G3 for the out-of-plane configuration (due to the particular symmetry in the flow field [4]). As a result of this delayed onset and the 90° rotation between the meridional planes of two successive bifurcation modules (which generate cross-sectional flow asymmetry), the value of δ_{Gn} for the out-of-plane configuration is about an order of magnitude smaller than that for the in-plane configuration. Figure 22 indicates that a high level of non-uniformity in the mass flow distribution is developed in just the first six generations of the geometrically symmetric unobstructed in-plane network.

Figure 22 shows that δ_{Gn} in any generation Gn is increased as a result of blockage anywhere in the network; this holds true even in generations which appear upstream of the location of the blockage. The increase in δ_{Gn} is found to be comparable in the two configurations, thus the order of magnitude disparity in δ_{Gn} between the in-plane and out-of-plane configurations, characteristic of unobstructed networks, can be significantly reduced in the presence of a single blockage. The symmetry in the flow field [4] is removed in the presence of a blockage and $\delta_{Gn} > 0$ from generation G1 onwards for both configurations. It is found that for the in-plane configuration, earlier occurrence of a blockage (i.e. at lower values of n) increases the values of δ_{Gn} at all generations. The dependence of δ_{Gn} on the position of the blockage is complex in the out-of-plane configuration, but certain generic trends exist. For example, the increase in δ_{Gn} (as compared to its value in the unobstructed network) is the greatest in the generation which lies immediately downstream of the location of the blockage and is the second greatest in the same generation where the blockage exists. It is also seen in Fig. 22 that, wherever the blockage occurs in the out-of-plane configuration, the difference in δ_{Gn} between the generation where the

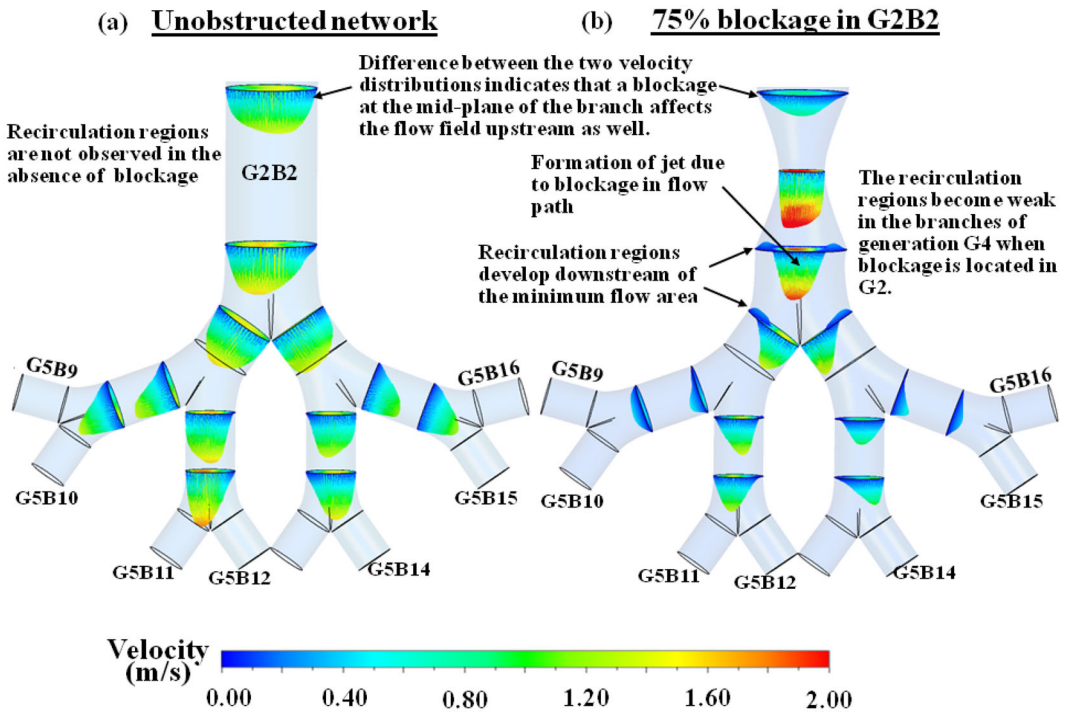

Fig. 20 The velocity distribution in branch G2B2 and in the branches of generation G3 and G4 originating from G2B2 of a six-generation network; in-plane configuration. **a** Unobstructed network, **b** 75% blockage in G2B2 (3D representation is formed by the envelope of velocity vectors drawn on each selected cross-sectional plane. The lengths of velocity vectors indicate magnitude which is also colour-coded)

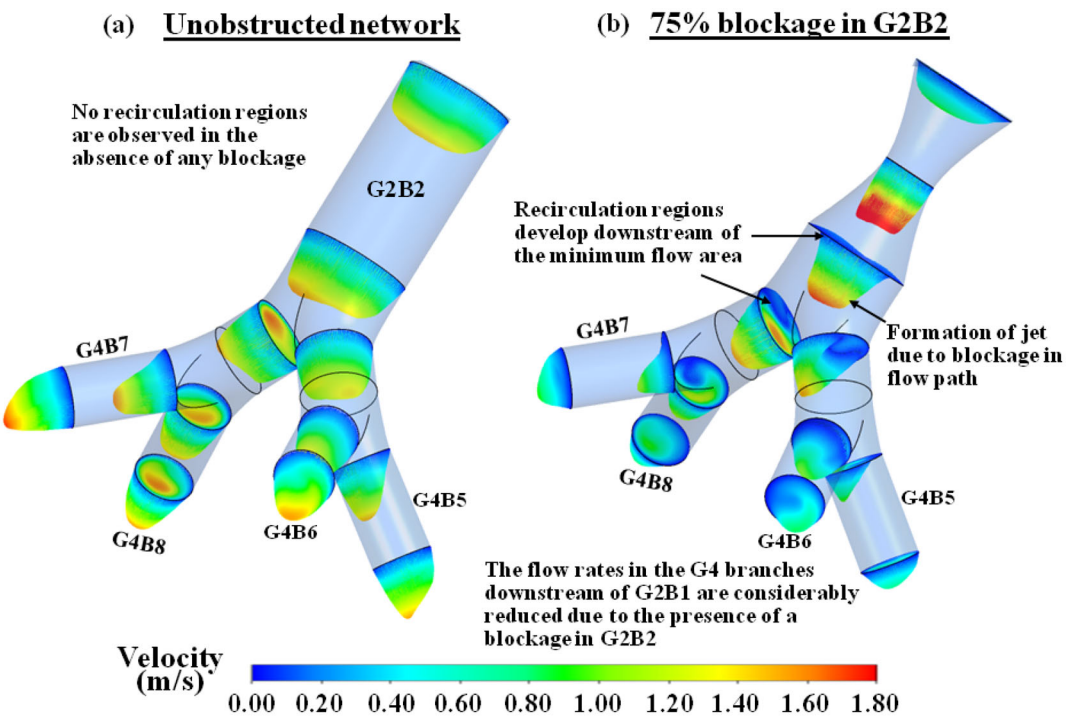

Fig. 21 The velocity distribution in branch G2B2 and in the branches of generation G3 and G4 originating from G2B2 of a six-generation network; out-of-plane configuration. **a** Unobstructed network, **b** 75% blockage in G2B2 (3D representation is formed by the envelope of velocity vectors drawn on each selected cross-sectional plane. The lengths of velocity vectors indicate magnitude which is also colour-coded)

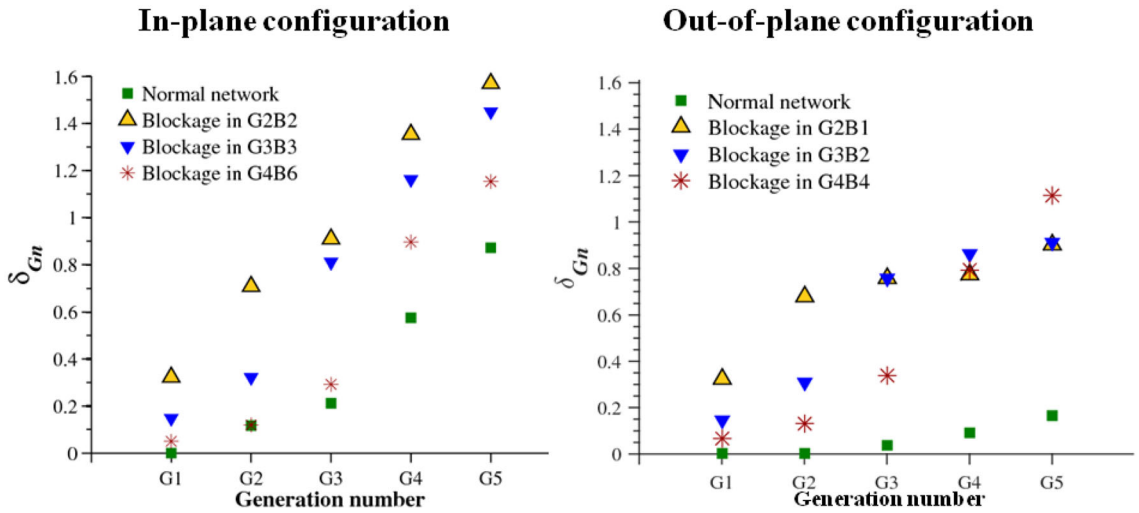

Fig. 22 Evolution of the degree of mass flow asymmetry δ_{Gn} with increasing generation number for different positions of blockage ($\varphi = 75\%$)

Table 6 A comparison of the effects of a blockage on the overall flow parameters in the in-plane and out-of-plane configurations

	Unobstructed network		75% Blockage in G2B2		75% Blockage in G3B3		75% Blockage in G4B6	
	In-plane	Out-of-plane	In-plane	Out-of-plane	In-plane	Out-of-plane	In-plane	Out-of-plane
$\dot{m}_{\text{inlet}}$ (10^{-5} kg/s)	25.34	25.44	22.34	22.53	23.94	24.07	24.86	24.90
δ_{G5}	0.871	0.167	1.570	0.899	1.450	0.913	1.153	1.114
$\delta_{G5,\text{rel}}$	–	–	0.803	4.383	0.665	4.467	0.324	5.671

blockage occurs and its immediately preceding generation is greater than the difference in δ_{Gn} between any other pair of consecutive generations.

Table 6 gives the overall mass flow rate, the degree of mass flow asymmetry at generation G5 (δ_{G5}) and its relative increase with respect to the unobstructed network ($\delta_{G5,\text{rel}} \equiv (\delta_{G5} - \delta_{G5,\text{unobstructed}})/\delta_{G5,\text{unobstructed}}$) for three positions of a 75% blockage in two branching configurations. As the blockage is shifted downstream from G2B2 to G3B3 to G4B6, δ_{G5} decreases in the in-plane configuration but increases in the out-of-plane configuration (though the absolute value of δ_{G5} for out-of-plane remains smaller than that for in-plane configuration). $\delta_{G5,\text{rel}}$ in the out-of-plane configuration is found to be an order of magnitude greater than that in the in-plane configuration. Thus, while it was established in Ref. [4] that the out-of-plane arrangement of branches fosters greater uniformity of flow distribution, the presence of a blockage affects this configuration to a much greater extent as compared to the in-plane arrangement, resulting in comparable degrees of non-uniformity in both.

In Table 7, values of $\delta_{Gn,L}$, $\delta_{Gn,R}$ (values of δ_{Gn} considering branches of generation Gn in sub-network L and R, respectively) and δ_{Gn} for a blockage in G2B2 are listed alongside the values of $\delta_{Gn,\text{unobstructed}}$. It was established in Ref. [4] that, for the in-plane configuration, the flow fields in sub-networks L and R are identical when the flow is unobstructed; therefore it can be concluded that, for flow in unobstructed in-plane network, the values of $\delta_{Gn,L}$, $\delta_{Gn,R}$ and δ_{Gn} are the same. Table 7, however, shows that $\delta_{Gn,L}$ and $\delta_{Gn,R}$ in the obstructed network are significantly different. While δ_{Gn} for the entire network is closer to the value of $\delta_{Gn,L}$ for a blockage in sub-network L (e.g. in G2B2), they are still quite different from one another. Although the sub-network R in the obstructed and unobstructed network is geometrically identical, the values of $\delta_{Gn,R}$ can appreciably change due to blockage. A rather large value of 0.333 for δ_{Gn} in generation G1, for a blockage in generation G2, shows that there can also be large upstream impact on the flow asymmetry. Thus, Table 7 establishes that a blockage does affect the asymmetry in the mass flow distribution in the entire network.

We have described in Sect. 2 why it is relevant to conceptually divide the out-of-plane network into four sub-networks L1, L2, R1 and R2 (the branch G2B2 in which a blockage is assumed belonging to L2). The fourfold symmetry in the out-of-plane configuration [4] results in identical values of $\delta_{Gn,L1}$, $\delta_{Gn,L2}$, $\delta_{Gn,R1}$, $\delta_{Gn,R2}$ and δ_{Gn} in the unobstructed network. However, a blockage removes all symmetry and all of the above-

Table 7 Variation of the degree of mass flow asymmetry in sub-networks L and R, and in the complete network, in the absence of any blockage and in the presence of a 75% blockage in G2B2; in-plane configuration

Generation	$\delta_{Gn,L}$	$\delta_{Gn,R}$	δ_{Gn}	$\delta_{Gn,unobstructed}$
G1	–	–	0.333	0
G2	0.657	0.124	0.723	0.115
G3	0.809	0.258	0.935	0.208
G4	1.239	0.695	1.397	0.568
G5	1.475	1.031	1.647	0.846

Table 8 Variation of the degree of mass flow asymmetry in sub-networks L1, L2, R1 and R2, sub-networks L and R, and in the complete network, in the absence of any blockage and in the presence of a 75% blockage in G2B2; out-of-plane configuration

Generation	$\delta_{Gn,L1}$	$\delta_{Gn,L2}$	$\delta_{Gn,L}$	$\delta_{Gn,R1}$	$\delta_{Gn,R2}$	$\delta_{Gn,R}$	δ_{Gn}	$\delta_{Gn,unobstructed}$
G1	–	–	–	–	–	–	0.322	0
G2	–	–	0.676	–	–	0.004	0.676	0
G3	0.089	0.071	0.756	0.060	0.060	0.064	0.756	0.038
G4	0.107	0.114	0.767	0.107	0.092	0.114	0.767	0.088
G5	0.156	0.270	0.881	0.213	0.199	0.213	0.895	0.164

mentioned values become unequal (Table 8). Nevertheless, it is found that the values of $\delta_{Gn,L1}$, $\delta_{Gn,L2}$, $\delta_{Gn,R1}$, $\delta_{Gn,R2}$ remain of the same order of magnitude as $\delta_{Gn,unobstructed}$, whereas the presence of blockage (in G2B2 in the example) significantly raises the values of $\delta_{Gn,L}$ and δ_{Gn}, the last two quantities being almost equal. The fact that $\delta_{Gn,L2} \approx \delta_{Gn,unobstructed}$ indicates that the significant change in mass flow rate of the blocked branch is nearly uniformly transmitted to its offspring branches (and their successive generations) in the out-of-plane configuration. The significant rise in the values of $\delta_{Gn,L}$ and δ_{Gn} is thus caused by the fact that the mass flow rates in L2 branches are all significantly reduced as compared to that in the branches of L1 (and the branches of R). In contrast to the out-of-plane configuration, the reduction in mass flow rate in a blocked branch in in-plane network is non-uniformly transmitted to its offspring branches and the non-uniformity may grow in successive generations (e.g. Fig. 5 vs Fig. 12). The sub-network-wise deconstruction of flow asymmetry and its generation-wise evolution (Tables 7 and 8) bring out this subtle but essential difference between in-plane and out-of-plane configurations.

7 Conclusion

A systematic three-dimensional (3D) computational study is performed to understand the effects of a blockage in a branching network (the geometries and dimensions used for the example computations being based on the first six generations of a model human bronchial tree). The consideration of a sufficiently large number of generations allows us to demonstrate the effects of blockages located at a number of different sites in the network. Both in-plane and 90° out-of-plane configurations are considered in order to determine the effect of the three-dimensional arrangement of the branches on the flow characteristics. It is established here that one-dimensional (1D) network models, consisting of the solution of simultaneous algebraic equations, are inadequate in describing either the qualitative or the quantitative aspects of the flow field for which a 3D computation is necessary. It is shown that the presence of a blockage makes three-dimensional alteration to the flow field, sometimes producing non-intuitive outcome. As an example, Fig. 16 shows that, in the unobstructed out-of-plane network, the mass flow rate in G3B1 is smaller than that in G3B2; a blockage in G2B1 reverses this distribution (i.e. the mass flow rate in G3B1 becomes greater than that in G3B2). Neither the existence of flow asymmetry in the original (geometrically symmetric) network nor the three-dimensional asymmetric modification of the flow field made even by a geometrically symmetric obstruction can be explained by a 1D model. Of course, a 1D model cannot differentiate between the in-plane and out-of-plane configurations.

Blockage in any one branch affects the flow in the entire network. Both downstream and upstream flow is affected; so flow at all outlets as well as that at the main inlet is altered (Figs. 7, 9, 10, 14, 16, 18). Qualitative and quantitative details of these changes are complex, and described in Sects. 4 and 6. Here we attempt to summarize a few general trends for an obstruction in any branch in sub-network L:

(i) Overall, the mass flow rate entering the network (i.e. in G0) decreases due to the presence of any blockage and the magnitude of decrease is progressively reduced as the location of blockage is shifted downstream. When a blockage of a fixed magnitude is shifted from one branch to any other branch of a given generation, the overall mass flow rate at the inlet of the network is found to remain nearly unaltered.

(ii) Blockage in any branch reduces the mass flow rates in its (downstream) daughter and granddaughter branches in subsequent generations, and in all (upstream) branches that fall along the flow path between the main inlet and the obstructed branch. The mass flow rates in the remaining branches of the sub-network L and all branches of sub-network R usually increase. [For the in-plane configuration, exception to the last rule may occur in the decrease in mass flow rates in the downstream branches following the sister of an obstructed branch and this may happen if the sister branch falls in the maximum flow path (e.g. G0B1–G5B11 in the in-plane configuration) of the original unobstructed network. For example, for obstruction in G2B1, mass flow rate in G3B3 and all its downstream branches *decrease* (Fig. 9). Similarly, for obstruction in G3B4, mass flow rate in G4B6 and all its downstream branches *decrease* (Fig. 10). Exceptions to the last rule are also found in out-of-plane configuration. For example, the mass flow rates in G3B4 and G4B7 decrease, instead of increasing, for blockage in any of G3B1 or G3B2 (Fig. 18). Similarly, the mass flow rates in G4B8, G4B12, G4B13 and G4B16 decrease, instead of increasing, for blockage in G4B3 or G4B4 (not shown pictorially).]

(iii) Out of all branches in the same generation of the obstructed branch, the maximum relative increase in the mass flow rate usually occurs in the sister branch of the obstructed branch. This principle may be violated if the sister of the obstructed branch falls in the maximum flow path of the original unobstructed network. An example of such exception is observed (though not pictorially shown) for a 75% obstruction in G4B5, where the increase in mass flow in the sister branch G4B6 is less than that in cousin sisters G4B7 and G4B8.)

(iv) A central jet-like flow structure in an obstructed branch, on flow division, creates high flow rates near the inner walls of the daughter branches and much reduced flow rates near the outer walls. Thus, in in-plane configuration, two granddaughters which are aligned with the obstructed branch receive high mass flow rates while two other granddaughters receive much reduced flow rate. In the out-of-plane configuration, the further division of flow into the granddaughters is caused by bifurcation ridges that are perpendicular to the ridge that causes flow division into the two daughters. Thus, the ratio of maximum to minimum flow rates in the four granddaughters is not far from 1 for out-of-plane configuration. However, if the jet is not aligned with the axis of the obstructed branch and the recirculating region is highly asymmetric, then the above generalizations may not apply (Fig. 19).

(v) Mass flow rates in branches in sub-network R are less affected than that in L which contains the blockage. (Exception: For obstruction in G2B1, the increase in mass flow rate in G2B3 is more than that in the sister branch G2B2, as shown in Fig. 9.)

(vi) The mass flow rate in a branch in sub-network R remains almost unaltered when a blockage of fixed extent is moved from one branch to another in the same generation G*n* of the sub-network L.

(vii) When a blockage of a fixed magnitude is shifted from one branch to its sister branch, it is found that the mass flow rates are significantly altered in the two sister branches and all branches that emanate from them; the mass flow rates through other branches remain almost unaltered.

(viii) As the extent of blockage at a given branch is increased, the changes in mass flow rates through all branches increase; the same additional change in percent blockage having greater effect as the value of percent blockage increases (Figs. 7 and 14).

The degree of mass flow asymmetry δ_{Gn} in any generation G*n* is increased as a result of blockage anywhere in the network; the relative increase $\left(\delta_{Gn} - \delta_{Gn,\text{unobstructed}}\right)/\delta_{Gn,\text{unobstructed}}$ being nearly an order of magnitude greater in out-of-plane configuration than that in in-plane configuration (Table 6). Thus, the order of magnitude disparity in δ_{Gn} between the in-plane and out-of-plane configurations, characteristic of unobstructed networks, can be significantly reduced in the presence of a single blockage. Other complexities and subtleties in the variation of asymmetry with location of blockage, extent of blockage and three-dimensional arrangement of branches are described in Sect. 6.

The complexity of the generalizations regarding the alteration in the flow field in a branching network due to the presence of a blockage, and of the exceptions to the rules, shows the necessity of the detailed three-dimensional computations such as the present one. Neither the quantitative information nor

all qualitative characteristics can be deduced from intuition or determined by simple one-dimensional models.

Compliance with ethical standards

Conflict of interest The authors declare that they have no conflict of interest.

Appendix: Mathematical formulation for the 1D model of the branching network

A realistic physical condition is implemented in the CFD solutions presented in the main body of the paper where it is assumed that the driving potential (Δp_{total} across the network) remains unaltered; then the mass flow rates at the inlet and in various branches need to be determined as part of the flow solution in the 1D model.

Unobstructed network

For a branching network comprising generations G0 to Gn, there are 2^n flow paths from the main inlet to the 2^n branches of generation Gn. The equation for the loss of total pressure along any of those flow paths may be written by applying the Hagen–Poiseuille equation sequentially across each branch that falls in that flow path. As an example, the equation for the flow path from G0B1 to GnB1 may be written as follows:

$$R_0 Q_{01} + R_1 Q_{11} + R_2 Q_{21} + \cdots + R_n Q_{n1} = \Delta p. \tag{A1}$$

Here, Q_{ij} is the flow rate in the jth branch of generation Gi which falls along the path for which the equation is written, Δp is the loss along that path in the 1D model, and R_i is the flow resistance in generation Gi and is given by the following expression:

$$R_i = \frac{128 \mu l_{\text{G}i}}{\pi d_{\text{G}i}^4} \tag{A2}$$

where l_{Gi} and d_{Gi} denote the length and diameter of a branch of generation Gi. Similarly, equations can be constructed for the loss of total pressure along the remaining $2^n - 1$ flow paths from G0B1 to GnBk (where $k = 2, 3, 4, \ldots 2^n$) in the unobstructed network. The system of 2^n simultaneous algebraic equations is solved to obtain the flow rates in the 2^n branches of generation Gn. The flow rates in all the other branches can then be determined by applying the flow conservation principle at each bifurcation. In the 1D model, since the viscous loss incurred along a path is obtained by sequentially applying the Hagen–Poiseuille formula to individual branches (where the static and total pressure drops are equal), the values of Δp and Δp_{total} along a path are equal. Therefore, the value of Δp in the 2^n equations is taken equal to the static pressure drop along each path obtained from the 3D computations.

Figure 23 shows that, for a fixed static pressure drop across the network, the mass flow rates obtained by the 1D model are significantly different (greater) from the results of 3D computations. Moreover, the 3D computations show that the mass flow rates in the various branches of the same generation can be significantly different. As an example, the 3D computations show that the difference between the minimum and maximum mass flow rates in generation G5 is as high as 85% of the average mass flow rate in G5. The 1D model predicts that the mass flow rates in all branches of the same generation of a geometrically symmetric network are equal. This shortcoming of the 1D model cannot be removed by improving the methodology of loss calculation (for example, by including, in future, a loss model for the flow in the bifurcation module [11]).

1D model in the presence of a blockage

When an obstruction occurs in any branch, additional terms accounting for the loss due to change of cross-sectional area in the obstructed branch needs to be included. For example, when an obstruction occurs in branch

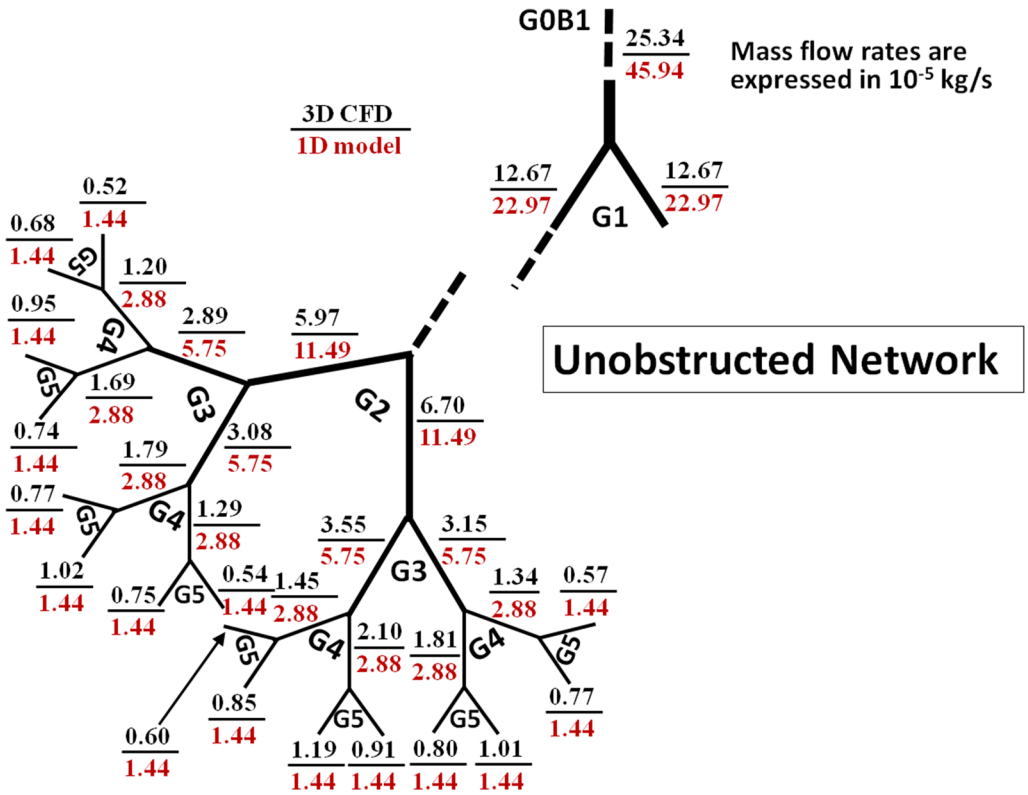

Fig. 23 A comparison of the mass flow distribution in the unobstructed G0–G5 network obtained from the 3D computations with those predicted by a 1D model for the same driving potential across the network

G2B1, the equation for the loss of total pressure along the flow path from G0B1 to GnB1 may be written as follows:

$$R_0 Q_{01} + R_1 Q_{11} + R_2 Q_{21} + R_2' Q_{21}^2 + R_3 Q_{31} + \cdots + R_n Q_{n1} = \Delta p. \tag{A3}$$

Here, R_i' is the minor loss coefficient accounting for the change of cross-sectional area in the obstructed branch. The value of R_i' is a function of the extent of blockage φ and branch length l_{Gi} [49]. Equation (A3) holds true for all flow paths containing the obstructed branch G2B1.

Since there are 2^n possible flow paths from G0 to Gn, we again obtain a system of 2^n simultaneous equations which need to be solved to obtain the flow rates in the 2^n branches of generation Gn, but the equations are nonlinear this time. In general, if a blockage occurs in generation Gm (where $0 < m \leq n$) of a G0–Gn network, then the nonlinear equation (A3) holds along 2^{n-m} flow paths, while equation (A1) holds for the remaining $(2^n - 2^{n-m})$ flow paths from G0B1 to GnBk(where $k = 1, 2, 3, \ldots 2^n$). An appropriate solution strategy is to be applied. In order to solve the system of equations, the value of Δp in the right-hand side of the equations is taken equal to the static pressure drop across the network obtained from the corresponding (same position and extent of blockage) 3D computations. A comparison of 3D and 1D computations in the presence of blockage is shown in Fig. 11 in the main body of the paper.

References

1. Guha, A.: Transport and deposition of particles in turbulent and laminar flow. Annu. Rev. Fluid Mech. **40**, 311–341 (2008)
2. Murray, J.J., Guha, A., Bond, A.: Overview of the development of heat exchangers for use in air-breathing propulsion pre-coolers. Acta Astronaut. **41**, 723–729 (1997)
3. Weibel, E.R.: Morphometry of the Human Lung. Springer, Berlin (1963)
4. Guha, A., Pradhan, K., Halder, P.K.: Finding order in complexity: a study of the fluid dynamics in a three-dimensional branching network. Phys. Fluids **28**(123602), 1–32 (2016)
5. Guha, A., Pradhan, K.: Secondary motion in three-dimensional branching networks. Phys. Fluids **29**(063602), 1–24 (2017)
6. Zhao, Y., Lieber, B.B.: Steady inspiratory flow in a model symmetric bifurcation. J. Biomech. Eng. **116**, 488–496 (1994)

7. Zhao, Y., Lieber, B.B.: Steady expiratory flow in a model symmetric bifurcation. J. Biomech. Eng. **116**, 318–323 (1994)
8. Zhao, Y., Brunskill, C.T., Lieber, B.B.: Inspiratory and expiratory steady flow analysis in a model symmetrically bifurcating airway. J. Biomech. Eng. **119**, 52–58 (1997)
9. Tadjfar, M., Smith, F.T.: Direct simulations and modelling of basic three-dimensional bifurcating tube flows. J. Fluid Mech. **519**, 1–32 (2004)
10. Kang, M.Y., Hwang, J., Lee, J.W.: Effect of geometric variations on pressure loss for a model bifurcation of the human lung airway. J. Biomech. **44**, 1196–1199 (2011)
11. Pradhan, K., Guha, A.: Fluid dynamics of a bifurcation. Int. J. Heat Fluid Flow **80**(108483), 1–29 (2019)
12. Liu, Y., So, R.M.C., Zhang, C.: Modeling the bifurcating flow in a human lung airway. J. Biomech. **35**, 465–473 (2002)
13. Comer, J.K., Kleinstreuer, C., Zhang, Z.: Flow structures and particle deposition patterns in double-bifurcation airway models. Part 1. Air flow fields. J. Fluid Mech. **435**, 25–54 (2001)
14. Wilquem, F., Degrez, G.: Numerical modeling of steady inspiratory airflow through a three-generation model of the human central airways. J. Biomech. Eng. **119**, 59–65 (1997)
15. Heistracher, T., Hofmann, W.: Flow and deposition patterns in successive airway bifurcations. Ann. Occup. Hyg. **41**, 537–542 (1997)
16. Leong, F.Y., Smith, K.A., Wang, C.H.: Secondary flow behavior in a double bifurcation. Phys. Fluids **21**, 043601 (2009)
17. Fresconi, F.E., Prasad, A.K.: Secondary velocity fields in the conducting airways of the human lung. J. Biomech. Eng. **129**, 722–732 (2007)
18. Nowak, N., Kakade, P.P., Annapragada, A.V.: Computational fluid dynamics simulation of airflow and aerosol deposition in human lungs. Ann. Biomed. Eng. **31**, 374–390 (2003)
19. Kleinstreuer, C., Zhang, Z.: An adjustable triple-bifurcation unit model for air-particle flow simulations in human tracheobronchial airways. J. Biomech. Eng. **131**, 021007 (2009)
20. Comerford, A., Förster, C., Wall, W.A.: Structured tree impedance outflow boundary conditions for 3D lung simulations. J. Biomech. Eng. **132**(8), 081002 (2010)
21. Ismail, M., Comerford, A., Wall, W.A.: Coupled and reduced dimensional modeling of respiratory mechanics during spontaneous breathing. Int. J. Numer. Methods Biomed. Eng. **29**(11), 1285–1305 (2013)
22. Kannan, R., Chen, Z.J., Singh, N., Przekwas, A., Delvadia, R., Tian, G., Walenga, R.: A quasi-3D wire approach to model pulmonary airflow in human airways. Int. J. Numer. Methods Biomed. Eng. **33**(7), e2838 (2017)
23. Pozin, N., Montesantos, S., Katz, I., Pichelin, M., Vignon-Clementel, I., Grandmont, C.: A tree-parenchyma coupled model for lung ventilation simulation. Int. J. Numer. Methods Biomed. Eng. **33**(11), e2873 (2017)
24. Pozin, N., Montesantos, S., Katz, I., Pichelin, M., Grandmont, C., Vignon-Clementel, I.: Calculated ventilation and effort distribution as a measure of respiratory disease and Heliox effectiveness. J. Biomech. **60**, 100–109 (2017)
25. Luo, H.Y., Liu, Y.: Modeling the bifurcating flow in a CT-scanned human lung airway. J. Biomech. **41**, 2681–2688 (2008)
26. Pourmehran, O., Gorji, T.B., Gorji-Bandpy, M.: Magnetic drug targeting through a realistic model of human tracheobronchial airways using computational fluid and particle dynamics. Biomech. Model. Mechanobiol. **15**, 1355–1374 (2016)
27. Li, Z., Kleinstreuer, C., Zhang, Z.: Simulation of airflow fields and microparticle deposition in realistic human lung airway models. Part I: airflow patterns. Eur. J. Mech. B Fluids **26**, 632–649 (2007)
28. Rahimi-Gorji, M., Pourmehran, O., Gorji-Bandpy, M., Gorji, T.B.: CFD simulation of airflow behavior and particle transport and deposition in different breathing conditions through the realistic model of human airways. J. Mol. Liq. **209**, 121–133 (2015)
29. Goodarzi-Ardakani, V., Taeibi-Rahni, M., Salimi, M.R., Ahmadi, G.: Computational simulation of temperature and velocity distribution in human upper respiratory airway during inhalation of hot air. Respir. Physiol. Neurobiol. **223**, 49–58 (2016)
30. Banko, A.J., Coletti, F., Schiavazzi, D., Elkins, C.J., Eaton, J.K.: Three-dimensional inspiratory flow in the upper and central human airways. Exp. Fluids **56**(117), 1–12 (2015)
31. Yang, X.L., Liu, Y., So, R.M.C., Yang, J.M.: The effect of inlet velocity profile on the bifurcation COPD airway flow. Comput. Biol. Med. **36**, 181–194 (2006)
32. Yang, X.L., Liu, Y., Luo, H.Y.: Respiratory flow in obstructed airways. J. Biomech. **39**, 2743–2751 (2006)
33. Longest, P.W., Vinchurkar, S., Martonen, T.: Transport and deposition of respiratory aerosols in models of childhood asthma. J. Aerosol Sci. **37**(10), 1234–1257 (2006)
34. Farkas, A., Balásházy, I.: Simulation of the effect of local obstructions and blockage on airflow and aerosol deposition in central human airways. J. Aerosol Sci. **38**, 865–884 (2007)
35. Soni, B., Thompson, D.: Effects of temporally varying inlet conditions on flow and particle deposition in the small bronchial tubes. Int. J. Numer. Methods Biomed. Eng. **28**, 915–936 (2012)
36. Pradhan, K., Guha, A.: Fluid dynamics of oscillatory flow in three-dimensional branching networks. Phys. Fluids **31**(063601), 1–29 (2019)
37. SolidWorks, Release: Dassault Systèmes. Solid Works Corporation, Waltham (2010)
38. ANSYS Academic Research, Release 15.0. ANSYS, Inc., Canonsburg, USA
39. Yin, Y., Choi, J., Hoffman, E.A., Tawhai, M.H., Lin, C.L.: Simulation of pulmonary air flow with a subject-specific boundary condition. J. Biomech. **43**, 2159–2163 (2010)
40. Barth, T.J., Jespersen, D.C.: The design and application of upwind schemes on unstructured meshes. Technical Report AIAA-89-0366, AIAA 27th Aerospace Sciences Meeting, Reno, Nevada (1989)
41. Mei, Y., Guha, A.: Implicit numerical simulation of transonic flow through turbine cascades on unstructured grids. Proc. Inst. Mech. Eng. Part A **219**, 35–47 (2005)
42. Guha, A., Young, J.B.: Time-marching prediction of unsteady condensation phenomena due to supercritical heat addition. In: Turbomachinery: Latest Developments in a Changing Scene, pp. 167–177. Institution of Mechanical Engineers, London, UK (1991). ISBN 0852987617
43. Guha, A.: Thermal choking due to nonequilibrium condensation. J. Fluids Eng. **116**, 599–604 (1994)
44. Roache, P.J.: Quantification of uncertainty in computational fluid dynamics. Ann. Rev. Fluid Mech. **29**, 123–160 (1997)

45. Celik, I.B., Ghia, U., Roache, P.J.: Procedure for estimation and reporting of uncertainty due to discretization in CFD applications. J. Fluids Eng. **130**(7), 078001 (2008)
46. Guha, A., Sengupta, S.: The fluid dynamics of work transfer in the non-uniform viscous rotating flow within a Tesla disc turbomachine. Phys. Fluids **26**(033601), 1–27 (2014)
47. Wright, D.: Human Physiology and Health. Heinemann Educational, Oxford (2000)
48. Jeong, J., Hussain, F.: On the identification of a vortex. J. Fluid Mech. **285**, 69–94 (1995)
49. Massey, B.: Mechanics of Fluids. 8th edn. Revised by Ward-Smith J., Taylor & Francis, New York, USA (2006)